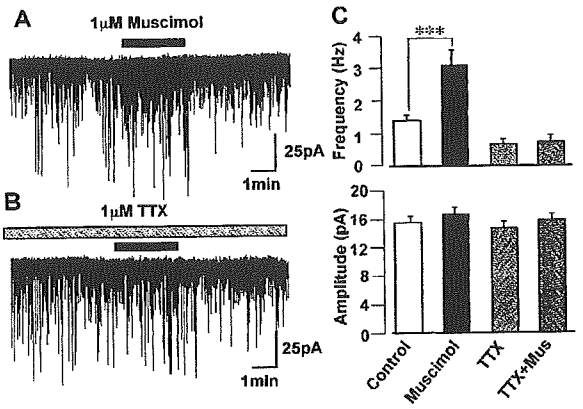

Fig. 5. Effect of tetrodotoxin (TTX) on the muscimol-induced facilitation of spontaneous EPSC frequency. (A and B) Typical current traces of spontaneous EPSCs observed before, during, and after application of 1 μM muscimol in the absence (A) or continued presence (B) of 1 μM TTX. (C) Histograms showing the mean affects of diazepam on the muscimol response. Data have been averaged from 5 neurons. Mus: muscimol; ***$P < 0.01$.

NKCC and/or the Cl^--HCO_3^- exchanger [26,38,39]. In immature and injured CNS neurons and sensory neurons, the Na–K–Cl cotransporter has an important role in raising the intracellular Cl^- concentration and hence causing GABA-induced depolarizations [27,35,39]. Furthermore, NKCC generates the Cl^- accumulation in glutamatergic nerve terminals projecting onto rat ventromedial hypothalamic neurons [23]. To investigate any contribution of NKCC to the muscimol-induced facilitation of release, we employed bumetanide, a potent blocker of NKCC [19].

The first application of muscimol in the presence of 10 μM bumetanide, a concentration which is specific for

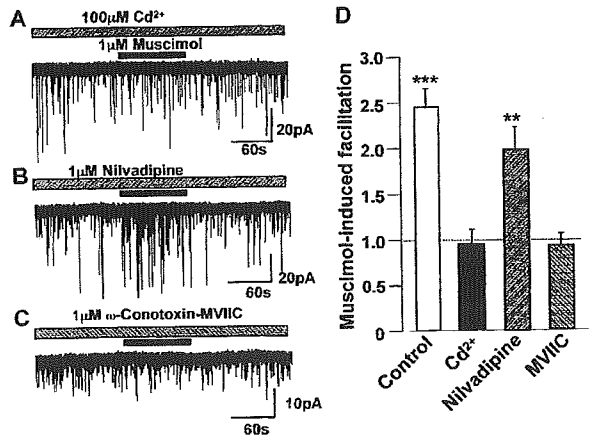

Fig. 6. Effects of Ca^{2+}-antagonists on the muscimol action. (A, B, and C) Typical current traces of spontaneous EPSCs observed before, during, and after application of 1 μM muscimol, all in the continued presence of 100 μM Cd (A), 1 μM nilvadipine (B), or 1 μM ω-conotoxin-MVIIC (C). The 3 traces were obtained from the same neuron. (D) Histograms showing the mean affects of the different Ca^{2+} channel blockers on the muscimol-induced enhancement of spontaneous EPSC frequency. Data have been averaged from 5 neurons. **$P < 0.01$, ***$P < 0.001$.

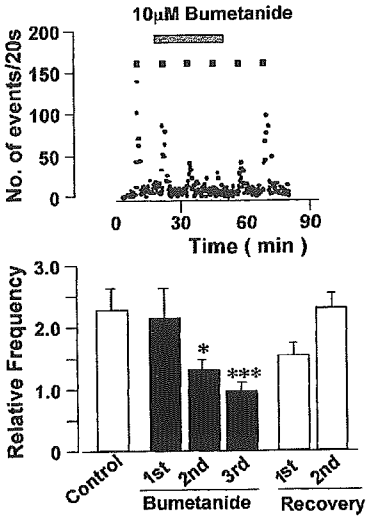

Fig. 7. Effect of bumetanide, an inhibitor of the Na–K–Cl cotransporter, on muscimol-induced facilitation of spontaneous EPSC frequency. Histograms show the relative facilitation of spontaneous EPSC frequency in response to muscimol alone, and then in response to 3 separate applications of muscimol in the continued presence of bumetinide, and again following bumetinide washout. Each column is the mean of data from 4 neurons and sEPSC frequency has been normalized to the control value. *$P < 0.05$, ***$P < 0.001$.

NKCC, induced nearly the same facilitatory effect as that observed in control conditions. However, subsequent applications of muscimol, in the continued presence of bumetanide, caused smaller amounts of facilitation and facilitation was absent on the third muscimol application (Fig. 7). The muscimol response slowly recovered back to control values after washing out bumetanide (Fig. 7). This result suggests that functional NKCC are present on these glutamatergic nerve terminals where they contribute to the maintenance of a high intraterminal Cl^- concentration.

4. Discussion

The present study demonstrates that $GABA_A$ receptors are present on glutamatergic nerve terminals projecting to noradrenergic neurons in the rat LC, and that their activation depolarizes these nerve terminals causing an increase in spontaneous glutamate release. This $GABA_A$-receptor-mediated depolarization seems to occur as a result of bumetanide-sensitive inwardly directed presynaptic NKCC transporters accumulating Cl^- in the terminals.

In mature CNS neurons, $GABA_A$ receptor activation generally hyperpolarizes the neuronal membrane as Cl^- ions enter the cell down their electrochemical gradient. In contrast, in immature neurons in the central and peripheral nervous system, $GABA_A$ receptor activation by exogenous or synaptically released GABA causes depolarization and neuronal excitation [6,27,33,36]. This depolarization can activate voltage-dependent Na^+ and Ca^{2+} channels to cause an increase in the postsynaptic intracellular Ca^{2+} concen-

tration [19,29,36,37]. The present study indicates that the $GABA_A$-receptor-induced depolarization activates voltage-dependent Na^+ channels causing an activation of voltage-dependent Ca^{2+} channels and facilitation of glutamate release. A similar sequence of events occurs following activation of presynaptic $GABA_A$ receptors on excitatory terminals projecting to rat ventral–medial hypothalamic neurons and for both glycine and $GABA_A$ receptors on glycinergic terminals projecting to sacral dorsal commissural neurons in the rat spinal cord [23–25].

Blockade of muscimol response by TTX may also suggest that the presynaptic $GABA_A$-receptor-mediated depolarization failed to directly activate presynaptic voltage-dependent Ca^{2+} channels. This is possibly because the amplitude of the depolarization was insufficient or because of the spatial distribution of the channels relative to the GABA receptors. N- and P/Q-type Ca^{2+} channels are reported to exist near the release site in the presynaptic terminals, and Ca^{2+} influx through these channels plays a key role in the transmitter release [32,46]. ω-Conotoxin-MVIIC, a blocker of these channels, reduced basal spontaneous EPSC frequency and abolished the facilitatory effect of muscimol. On the other hand, L-type Ca^{2+} channels have been reported to be localized at presynaptic boutons some distance from the neurotransmitter release site and hence Ca^{2+} influx through L-type Ca^{2+} channels does not directly trigger neurotransmitter release [32]. L-type Ca^{2+} channels may, however, play some role in propagating action potentials down to the release sites [30,34]. Thus, the reduction of the basal spontaneous EPSC frequency by the L-type channel blocker, nilvadipine, may be due to a decrease in Ca^{2+}-mediated action potentials which then propagate to the release sites. Niveldipine did not, however, affect the muscimol-induced facilitation, suggesting that this response may be localized closer to the release sites.

Direct iontophoretic application of GABA has an inhibitory effect on the LC neurons [45]. Thus, before starting this study, we hypothesized that GABA might reduce the EPSC frequency. But, the present results are contrary to these expectations. One possible clinical relation to our present results concerns the role of the LC in anxiety and panic disorders. Noradrenaline release from the LC enhances anxiety [9,13,14,16] and treatment for this illness often involves the benzodiazepines. A reduction in LC activity due to a potentiation of postsynaptic LC $GABA_A$ receptors is thought to contribute to their anti-anxiety actions [14,15]. However, depression, agitated toxic psychosis, hypomanic and manic behavior, increased anxiety, increased hostility and paradoxical rage reactions have all been reported to be caused by the benzodiazepines [18]. Our current results suggest that the benzodiazepine enhances the glutamate release by muscimol onto LC neurons. That may increase noradrenaline release from LC neurons. Furthermore, there are several reports suggesting that systemic or intracerebroventricular injection of GABA enhances noradrenaline synthesis and utilization rate [2,11]. Scatton and Serrano [40] reported that systemic administration of muscimol enhanced the catechol current measured in the LC by in vivo voltammetry. GABA is also reported to increase evoked noradrenaline release from rat cortical slices [47]. An increase of glutamate release to the LC neurons by GABA might be one mechanism contributing to these excitatory actions of GABA and muscimol on LC activity and to the paradoxical benzodiazepine-induced enhancement of anxiety.

Acknowledgments

We thank Dr. A. Moorhouse for discussion and editing of the manuscript. This work was supported by research grants from the Ministry of Education, Culture, Sports, Science and Technology, Japan (15016082, 15650076 and 15390065 to J.N.). This work was also supported by CREST, JST.

References

[1] N. Akaike, A.J. Moorhouse, Techniques: applications of the nerve-bouton preparation in neuropharmacology, Trends Pharmacol. Sci. 24 (2003) 44–47.
[2] S. Arbilla, S.Z. Langer, Facilitation by GABA of the potassium evoked release of ^{3}H-noradrenaline from the rat occipital cortex, Naunyn-Schmiedeberg's Arch. Pharmacol. 306 (1979) 161–168.
[3] J. Arima, C. Kubo, H. Ishibashi, N. Akaike, α_2-Adrenoceptor-mediated potassium currents in acutely dissociated rat locus coeruleus neurons, J. Physiol. 508 (1998) 57–66.
[4] G. Aston-Jones, F.E. Bloom, Activity of norepinephrine-containing locus coeruleus neurons in behaving rats anticipates fluctuations in the sleep–waking cycle, J. Neurosci. 18 (1998) 67–886.
[5] G. Aston-Jones, J. Rajkowski, J. Cohen, Locus coeruleus and regulation of behavioral flexibility and attention, Prog. Brain Res. 126 (2000) 165–182.
[6] K. Ballanyi, P. Grafe, An intracellular analysis of γ-aminobutyric-acid-associated ion movements in rat sympathetic neurons, J. Physiol. 365 (1985) 41–58.
[7] C.W. Berridge, B.D. Waterhouse, The locus coeruleus–noradrenergic system; modulation of behavioral state and state-dependent cognitive processes, Brain Reserch Reviews 42 (2003) 33–84.
[8] P.J. Charlety, K. Chergui, H. Akaoka, C.F. Saunier, M. Buda, G. Aston-Jones, G. Chouvet, Serotonin differentially modulates responses mediated by specific excitatory amino acid receptors in the rat locus coeruleus, Eur. J. Neurosci. 5 (1993) 1024–1028.
[9] D.S. Charney, G.R. Heninger, A. Breier, Noradrenergic function in panic anxiety. Effects of yohimbine in healthy subjects and patients with agoraphobia and panic disorder, Arch. Gen. Psychiatry 41 (8) (1984 (Aug.)) 751–763.
[10] G. Chen, P.Q. Trombley, A.N. van den Pol, Excitatory actions of GABA in developing rat hypothalamic neurons, J. Physiol. (London) 494 (1996) 451–464.
[11] T. Dennis, O. Curet, T. Nishikawa, B. Scatton, Further evidence for, and nature of, the facilitatory GABAergic influence on central noradrenergic transmission, Naunyn-Schmiedeberg's Arch. Pharmacol. 331 (1985) 225–234.
[12] M. Ennis, G. Aston-Jones, GABA-mediated inhibition of locus coeruleus from the dorsomedial rostral medulla, J. Neurosci. 9 (1989) 2973–2981.
[13] S.L. Foote, F.E. Bloom, G. Aston-Jones, Nucleus locus coeruleus: new

evidence of anatomical and physiological specificity, Physiol. Rev. 63 (1983) 844–914.
[14] A.W. Goddard, S.W. Woods, D.S. Charney, A critical review of the role of norepinephrine in panic disorder: focus on its interaction with serotonin, in: H.G.M. Westenberg, et al., (Eds.), Advances in the Neurobiology of Anxiety Disorders, Wiley, New York, 1996, pp. 107–137.
[15] A.W. Goddard, T. Brouette, A. Almai, Early coadministration of clonazepam with sertraline for panic disorder, Arch. Gen. Psychiatry 58 (2001) 681–686.
[16] J.M. Gorman, Ventilatory physiology of patients with panic disorder, Arch. Gen. Psychiatry 45 (1988) 31–39.
[17] T.G. Hales, M.J. Sanderson, A.C. Charles, GABA has excitatory actions on GnRH-secreting immortalized hypothalamic (GT1-7) neurons, Neuroendocrinology 59 (1994) 297–308.
[18] R.C. Hall, S. Zisook, Paradoxical reactions to benzodiazepines, Br. J. Clin. Pharmacol. 11 (Suppl. 1) (1981) 99S–104S.
[19] M. Haas, Properties and diversity of (Na–K–Cl) cotransporters, Annu. Rev. Physiol. 51 (1989) 443–557.
[20] D.R. Hillyard, V.D. Monje, I.M. Mintz, B.P. Bean, L. Nadasdi, J. Ramachandran, G. Miljanich, A. Azimi-Zoonooz, J.M. McIntosh, L.J. Cruz, J.S. Imperial, B.M. Olivera, A new conus pepetide ligand for mammalian presynaptic Ca^{2+} channels, Neuron 9 (1992) 69–77.
[21] J.A. Hobson, R.W. McCarley, P.W. Wyzinski, Sleep cycle oscillation: reciprocal discharge by two brainstem neuronal groups, Science 189 (1975) 55–58.
[22] H. Ishibashi, Y. Murai, N. Akaike, Effect of nilvadipine on the voltage-dependent Ca^{2+} channels in rat hippocampal CA1 pyramidal neurons, Brain Res. 813 (1998) 121–127.
[23] I.-S. Jang, H.-J. Jeong, N. Akaike, Contribution of the Na–K–Cl cotransporter on $GABA_A$ receptor-mediated presynaptic depolarization in excitatory nerve terminals, J. Neurosci. 21 (2001) 5962–5972.
[24] I.-S. Jang, H.-J. Jeong, S. Katsurabayashi, N. Akaike, Functional roles of presynaptic $GABA_A$ receptors on glycinergic nerve terminals in the rat spinal cord, J. Physiol. 541 (2002) 423–434.
[25] H.-J. Jeong, I.-S. Jang, A.J. Moorhouse, N. Akaike, Activation of presynaptic glycine receptors facilitates glycine release from presynaptic terminals synapsing onto rat spinal sacral dorsal commissural nucleus neurons, J. Physiol. 550 (Pt. 2) (2003 (Jul. 15)) 373–383.
[26] K. Kaila, Ionic basis of $GABA_A$ receptor channel function in the nervous system, Prog. Neurobiol. 42 (1994) 489–537.
[27] Y. Kakazu, N. Akaike, S. Komiyama, J. Nabekura, Regulation of intracellular chloride by cotransporters in developing lateral superior olive neurons, J. Neurosci. 19 (1999) 2843–2851.
[28] E. Kumamoto, Y. Murata, Characterization of GABA current in rat septal cholinergic neurons in culture and its modulation by metal cations, J. Neurophysiol. 74 (1995) 2012–2027.
[29] X. Leinekugel, V. Tseeb, Y. Ben-Ari, P. Bregestovski, Synaptic $GABA_A$ activation induces Ca^{2+} rise in pyramidal cells and interneurons from rat hippocampal slices, J. Physiol. (London) 487 (1995) 319–329.
[30] F.M. Lu, K. Kuba, Synchronous and asynchronous exocytosis induced by subthreshold high K^+ at Cs^+-loaded terminals of rat hippocampal neurons, J. Neurophysiol. 87 (2002) 1222–1233.
[31] S. Marinelli, C.W. Vaughan, M.J. Christie, M. Connor, Capsaicin activation of glutamatergic synaptic transmission in the rat locus coeruleus in vitro, J. Physiol. 543 (2002) 531–540.
[32] R.J. Miller, Multiple calcium channels and neuronal function, Science 235 (1987) 46–52.
[33] U. Misgeld, R.A. Deisz, H.U. Dodt, H.D. Lux, The role of chloride transport in postsynaptic inhibition of hippocampal neurons, Science 232 (1986) 1413–1415.
[34] N. Murakami, H. Ishibashi, S. Katsurabayashi, N. Akaike, Calcium channel subtypes on single GABAergic presynaptic terminal projecting to rat hippocampal neurons, Brain Res. 951 (2002) 121–129.
[35] J. Nabekura, T. Ueno, A. Okabe, A. Furuta, T. Iwaki, C. Shimizu-Okabe, A. Fukuda, N. Akaike, Reduction of KCC2 expression and $GABA_A$ receptor-mediated excitation after in vivo axonal injury, J. Neurosci. 22 (2002) 4412–4417.
[36] K. Obrietan, A.N. van den Pol, GABA neurotransmission in the hypothalamus: developmental reversal from Ca^{2+} elevating to depressing, J. Neurosci. 15 (1995) 5065–5077.
[37] D.F. Owens, L.H. Boyce, B.E. Davis, A.R. Kriegstein, Excitatory GABA responses in embryonic and neonatal cortical slices demonstrated by gramicidin perforated-patch recordings and calcium imaging, J. Neurosci. 16 (1996) 6414–6423.
[38] M.D. Plotkin, E.Y. Snyder, S.C. Hebert, E. Delpire, Expression of the Na–K–2Cl cotransporter is developmentally regulated in postnatal rat brain: a possible mechanism underlying GABA's excitatory role in immature brain, J. Neurobiol. 33 (1997) 781–795.
[39] J.M. Russell, Sodium–potassium–chloride cotransport, Physiol. Rev. 80 (2000) 211–276.
[40] B. Scatton, A. Serrano, GABA mimetics increase extracellular DOPAC (as measured by in vivo voltammetry) in the rat locus coeruleus, Naunyn-Schmiedeberg's Arch. Pharmacol. 332 (1986) 380–383.
[41] I. Segev, Computer study of presynaptic inhibition controlling the spread of action potentials into axon terminals, J. Neurophysiol. 63 (1990) 987–998.
[42] T. Shirasaki, K. Aibara, N. Akaike, Direct modulation of $GABA_A$ receptor by intracellular ATP in dissociated nucleus tractus solitarii neurones of rat, J. Physiol. 449 (1992) 551–572.
[43] N. Singewald, A. Philippu, Release of neurotransmitters in the locus coeruleus, Prog. Neurobiol. 56 (1998) 237–267.
[44] G.J. Stuart, S.J. Redman, The role of $GABA_A$ and $GABA_B$ receptors in presynaptic inhibition of Ia EPSPs in cat spinal motoneurones, J. Physiol. 449 (1992) 551–572.
[45] S.T. Szabo, P. Blier, Serotonin (1A) receptor ligands act on norepinephrine neuron firing through excitatory amino acid and GABA(A) receptors: a microiontophoretic study in the rat locus coeruleus, Synapse 42 (2001) 203–212.
[46] T. Takahashi, A. Momiyama, Different types of calcium channels mediate central synaptic transmission, Nature 366 (1993) 156–158.
[47] H.D. Taube, K. Starke, E. Borowski, Presynaptic receptor systems on the noradrenergic neurons of the rat brain, Naunyn-Schmiedeberg's Arch. Pharmacol. 299 (1977) 123–141.
[48] S. Uchida, E. Noda, Y. Kakazu, Y. Mizoguchi, N. Akaike, J. Nabekura, Allopregnanolone enhancement of GABAergic transmission in rat medial preoptic area neurons, Am. J. Physiol.: Endocrinol. Metab. 283 (2002) E1257–E1265.
[49] U. Ungerstedt, Stereotaxic mapping of the monoamine pathways in the rat brain, Acta Physiol. Scand. 367 (1971) 1–48 (Suppl.).
[50] J.T. Williams, R.A. North, Catecholamine inhibition of calcium action potentials in rat locus coeruleus neurons, Neuroscience 14 (1985) 103–109.

Available online at www.sciencedirect.com
SCIENCE DIRECT®
Cellular Immunology 231 (2004) 20–29
Cellular Immunology
www.elsevier.com/locate/ycimm

Exosomes secreted from monocyte-derived dendritic cells support in vitro naive CD4$^+$ T cell survival through NF-κB activation☆

Kotaro Matsumoto[a,1], Takashi Morisaki[a], Hideo Kuroki[a], Makoto Kubo[a], Hideya Onishi[a], Katsuya Nakamura[a], Chihiro Nakahara[a], Hirotaka Kuga[a], Eishi Baba[a], Masafumi Nakamura[a], Kazuho Hirata[b], Masao Tanaka[c], Mitsuo Katano[a,*]

[a] *Department of Cancer Therapy and Research, Graduate School of Medical Sciences, Kyushu University, Fukuoka, Japan*
[b] *Department of Anatomy and Cell Biology, Graduate School of Medical Sciences, Kyushu University, Fukuoka, Japan*
[c] *Department of Surgery and Oncology, Graduate School of Medical Sciences, Kyushu University, Fukuoka, Japan*

Received 9 August 2004; accepted 4 November 2004
Available online 11 January 2005

Abstract

We investigated the effect of exosomes secreted from human monocyte-derived dendritic cells (Mo-DCs), which are generated from PBMCs in response to treatment with GM-CSF and IL-4, on naive CD4$^+$ T cell survival in vitro. Exosomes isolated from culture supernatants of Mo-DCs (>90% purity) were purified with anti-HLA-DP, -DQ, -DR-coated paramagnetic beads. Purified exosomes prolonged the survival of naive CD4$^+$ T cells (>98% purity) in vitro. Treatment with neutralizing mAb against HLA-DR significantly decreased the supportive effect of purified exosomes on CD4$^+$ T cell survival. Exosomes increased nuclear translocation of NF-κB in naive CD4$^+$ T cells, and NF-κB activation was significantly suppressed by anti-HLA-DR mAb or NF-κB inhibitor pyrrolidine dithiocarbamate (PDTC). In addition, PDTC inhibited the effect of exosomes on naive CD4$^+$ T cell survival. Thus, exosomes secreted by Mo-DCs appear to support naive CD4$^+$ T cell survival via NF-κB activation induced by interaction of HLA-DR and TCRs.

Keywords: Human monocyte-derived dendritic cells; Multivesicular body; Small membrane vesicle; TCR and MHC interaction

1. Introduction

Prolonged survival of naive CD4$^+$ T cells requires direct contact with self-MHC class II ligands in vivo [1–3]. CD8$^+$ T cells also require exposure to specific self-MHC class I proteins for prolonged survival [4]. Thus, interaction between TCR and MHC molecules plays an important role in supporting naive T cell survival in vivo [5,6]. However, there are few reports concerning the role of TCR and MHC interaction in short-term survival of naive CD4$^+$ T cells in vitro [7].

Exosomes were initially described as microvesicles containing 5′-nucleotidase activity and released from neoplastic cell lines [8,9]. Electron microscopy has shown that exosomes have a characteristic saucer-like morphology of a flattened sphere limited by a lipid bilayer. They range from 30 to 100 nm in diameter [10]. The most common procedure for purifying exosomes from cell-culture supernatants involves a series of centrifugations to remove dead cells and large debris, followed by a final high-speed ultracentrifugation to pellet the exosomes [11,12]. It is generally believed that exosomes are

☆ This work is supported in part by a Grant for Scientific Research (13470240) from the Ministry of Education, Science and Culture, Japan.
* Corresponding author. Fax: +81 92 642 6221.
E-mail address: mkatano@tumor.med.kyushu-u.ac.jp (M. Katano).
[1] Present address: Department of Surgery and Oncology, Graduate School of Medical Sciences, Kyushu University, Fukuoka, Japan.

0008-8749/$ - see front matter © 2004 Elsevier Inc. All rights reserved.
doi:10.1016/j.cellimm.2004.11.002

membrane vesicles that form within late endocytic compartments, multivesicular bodies (MVBs), and are secreted upon fusion of these compartments with the plasma membrane of living cells. As a result, all exosomal proteins reported up to now have been found in the cytosol, in the membrane of endocytic compartments, or at the plasma membrane. Various cell types secrete exosomes. APCs such as dendritic cells (DCs)[2] and B cells also secrete exosomes. Recent advances in biotechnology have made it possible to generate DC-like cells, monocyte-derived DCs (Mo-DCs), in vitro from PBMCs upon treatment with GM-CSF and IL-4 [13], and Mo-DCs secrete exosomes [14]. MHC class II proteins are very abundant in exosomes from Mo-DCs as well as other APCs [15]. In addition, APC-derived exosomes contain specific proteins, such as CD86 and integrins, which are involved in antigen presentation, suggesting a role of exosomes in T cell stimulation [16–18]. In fact, it has been shown that EBV-transformed B cell-derived exosomes stimulate human $CD4^+$ T cell clones in an antigen-specific manner [10]. T cell stimulation by exosomes produced by rat mast cells engineered to express mouse or human MHC class II proteins has been reported [19]. Interestingly, exosomes produced by tumor peptide-pulsed DCs induce T cell-dependent tumor rejection in vivo [14].

NF-κB is a transcription factor that is activated in T cells by interaction between TCRs and MHC class I or class II proteins [20–22] and has been shown to play an important role in the expression of anti-apoptotic genes [23]. In most resting cells, NF-κB is located in the cytoplasm as a heterodimer of the structurally related proteins p50, p52, RelA, c-Rel, and RelB. All of these are noncovalently associated with the cytoplasmic inhibitor IκB [24]. The most common NF-κB is the p65/p50 heterodimer. Activation of NF-κB is preceded by phosphorylation of IκB by IκB kinase, which is followed by proteolytic removal of IκB and movement of NF-κB to the nucleus. Nuclear translocation of NF-κB is thought to reflect its activation [25]. Zheng et al [26] reported a critically important function of NF-κB in TCR-induced regulation of $CD4^+$ T cell survival in p50−/− cRel−/− mice. In addition, survival of antigen-stimulated T cells requires NF-κB-mediated inhibition of p73 expression [22]. Thus a role of NF-κB in T cell survival appears to be important. However, a role of the NF-κB-activating pathway in naive $CD4^+$ T cell survival has not been identified in human cells.

Here, we report for the first time that Mo-DC-derived exosomes support naive $CD4^+$ T cell survival in vitro through interaction between TCRs and human leukocyte antigen (HLA)-DR, and that TCR-dependent NF-κB activation may contribute to this survival.

2. Materials and methods

2.1. Reagents

Pyrrolidine dithiocarbamate (PDTC), an inhibitor of NF-κB nuclear translocation, was purchased from Sigma Chemical (Deisenhofen, Germany).

2.2. Preparation of human Mo-DCs and naive $CD4^+$ T cells

Mo-DCs were generated from the adherent fraction of PBMCs from healthy volunteers, as previously described but with minor modifications [13]. Briefly, PBMCs were isolated from heparinized peripheral blood by Ficol–Paque (Life Technologies, Gaithersburg, MD, USA) density gradient centrifugation. PBMCs were resuspended in RPMI 1640 basal medium (Sanko Pure Chemicals, Tokyo Japan) supplemented with 1% human albumin (Mitsubishi Pharma, Osaka, Japan), 100 μg/ml penicillin (Meijiseika, Tokyo, Japan), and 100 μg/ml streptomycin (Meijiseika) (RPMI medium), plated at a density of 2×10^6 cells/ml, and allowed to adhere overnight at 37 °C in 24-well plates (Nalge Nunc International, Chiba, Japan). Nonadherent cells were removed, and adherent cells were cultured in RPMI medium containing GM-CSF (100 ng/ml, North China Pharmaceutical Group, Shijiazhuang, China) and IL-4 (50 ng/ml, Osteogenetics, Wurzburg, Germany). On day 7, nonadherent fractions were collected as Mo-DCs. Mo-DCs were further purified by negative selection with magnetic beads coated with mouse monoclonal anti-CD2, anti-CD3, and anti-CD19 antibodies (Dynabeads, Dynal Biotech, Oslo, Norway). This depletion procedure yielded over 90% $CD14^-$, $CD80^+$, and $HLA\text{-}DR^+$ Mo-DCs as assessed by fluorescence-activated cell sorting (FACS) (FACS Calibur flow cytometer, Becton–Dickinson Immunocytochemistry Systems, Franklin Lakes, NJ, USA) and analyzed with CELLQuest software (Becton–Dickinson).

Seven days after the initial culture of nonadherent cells, PBMCs were collected again from the same healthy volunteer. $CD4^+$ T cells were purified from fresh human PBMCs with a CD4-positive isolation kit (Dynabeads, Dynal Biotech) according to the manufacturer's instructions. This positive-selection process yielded over 98% $CD4^+$ T cells.

Fresh $CD4^+$ T cells and Mo-DCs isolated from the same healthy volunteer were used throughout this study.

[2] *Abbreviations used:* DC, dendritic cell; Mo-DC, monocyte-derived dendritic cell; PDTC, pyrrolidine dithiocarbamate; MVB, multivesicular body; CB, cacodylate buffer; MW, molecular weight; FSC, forward scatter; SSC, side scatter.

2.3. Exosome isolation and purification

Mo-DCs were generated from PBMCs with GM-CSF and IL-4 as described above. Seven days after the initiation of culture, Mo-DC culture supernatants were collected. Exosomes were isolated as previously described but with minor modifications [11,12]. Culture supernatants were centrifuged at 300*g* for 5 min and then at 1200*g* for 20 min to eliminate cells and debris. Cell-free supernatants were clarified through a 0.2-μm filter (Sartorius AG, Goettingen, Germany) to reduce the number of contaminating large vesicles shed from the plasma membrane. The clarified supernatant was subsequently concentrated through a 100-kDa membrane (YM-100, Microcon, Millipore, Billerica, MA, USA). In some experiments, this concentration procedure was repeated five times with PBS (Wako Pure Chemical Industries, Osaka, Japan) to eliminate the original culture supernatant. The concentrated materials were resuspended in RPMI medium at the original volume of the supernatant. This preparation was denoted crude exosomes.

Exosomes were further purified with human anti-HLA-DP, -DQ, or -DR-coated paramagnetic beads (average size: 4.5 μm, Dynal). Briefly, human anti-HLA-DP, -DQ, or -DR-coated paramagnetic beads were washed with PBS. And 1.0×10^6 DC-derived exosomes were mixed with 1.0×10^6 paramagnetic beads. The mixture was incubated at 4 °C for 24 h on a rotating plate, and the beads were washed twice on a magnetic rack with PBS containing 3% BSA (Sigma) and 0.1% NaN_3 (Sigma) (referred to as FACS buffer) to eliminate unbound or excess exosomes. Finally, exosomes coupled to the beads were resuspended in RPMI medium at the original volume of the exosome-containing medium. This preparation was denoted purified exosomes.

2.4. Naive $CD4^+$ T cell culture

$CD4^+$ T cells were suspended at a cell density of 1.0×10^6/ml, and 1.5×10^5 $CD4^+$ T cells were plated in a 96-well flat-bottomed culture plate (150 μl) and cultured at 37 °C for the indicated times. In an experiment using separated cell-culture system, $CD4^+$ T cells (1.5×10^6 cells) were cultured with Mo-DCs (1.5×10^5 cells) in 1.5 ml of RPMI medium or were cultured separately in RPMI medium (1.5 ml) with a 0.4-μm separated cell-culture system (Becton–Dickinson). Cellular viability and the number of $CD4^+$ T cells were determined by trypan blue dye exclusion and a cell counter (CDA-500, Sysmex Mundelin, IL, USA), respectively. T cells and DCs were easily distinguishable with each cell size using a cell counter.

2.5. Blocking assay for MHC class II molecules

To examine the effect of MHC class II proteins on Mo-DCs or of exosome preparations on naive $CD4^+$ T cell survival, Mo-DCs (1.0×10^5 cells/ml), crude exosomes, or purified exosomes prepared from 1×10^5 Mo-DC/ml were preincubated with anti-MHC class II mAb (4 μg/ml, Diaclone Research Besaucon, France) at 37 °C for 1 h, and $CD4^+$ T cells (1.0×10^6 cells/ml) were added and cultured at 37 °C for 4 days. Isotype-matched IgG1 mAb was used as a control.

2.6. FACS analysis

A 10× concentrate of crude exosomes (100 μl) was mixed with 100 μl FITC-conjugated anti-HLA-DR mAb and PE-conjugated anti-CD86 mAb. After a 30-min incubation at 4 °C, the samples were diluted with FACS buffer, and the fluorescence intensities of the exosome preparations were measured with a FACS Calibur flow cytometer and were analyzed with CELLQuest software.

Purified exosomes were prepared with human anti-HLA-DP, -DQ, or -DR-coated paramagnetic beads as described above. Purified exosomes (10 μl) were suspended in 100 μl FACS buffer, mixed with FITC-conjugated anti-HLA-DR mAb (10 μl) and PE-conjugated anti-CD86 mAb (10 μl), and incubated at 4 °C for 30 min. The samples were washed twice on a magnetic rack with FACS buffer, followed by reconstitution of the bead pellets in buffer containing 1% formaldehyde. Stained and fixed exosome-coupled beads were analyzed on a FACS Calibur flow cytometer with CELLQuest software.

2.7. Electrophoretic mobility shift assay

NF-κB activity in nuclei isolated from naive $CD4^+$ T cells was determined by electrophoretic mobility shift assay (EMSA). Extraction of nuclear proteins and EMSA were performed as described previously [27]. Briefly, 5 μg of nuclear protein was incubated for 30 min at room temperature with binding buffer (20 mM Hepes–NaOH, pH 7.9, 2 mM EDTA, 100 mM NaCl, 10% glycerol, and 0.2% NP-40), poly(dI–dC), and ^{32}P-labeled double-stranded oligonucleotide containing the NF-κB binding motif (Promega, Madison, WI, USA). The sequence of the double-stranded oligomer used for EMSA is as follows: 5′-AGTTGAGGGGACTTTCCC AGGC-3′ (sense strand). The reaction mixtures were loaded on a 4% polyacrylamide gel and electrophoresed with running buffer 0.25× TBE. After the gel was dried, DNA–protein complexes were visualized by autoradiography.

2.8. Electron microscopy

Exosome-bead complexes were fixed in 3% glutaraldehyde in 0.1 M cacodylate buffer (CB) at pH 7.3 for 3 h at 4 °C and washed in 0.1 M CB. The complexes were resuspended and embedded in 4% agar [28]. After the

agar was cut into 1-mm^3 pieces, the pieces were fixed in 1% osmium tetroxide in 0.1 M CB overnight and washed in distilled water. The specimens were dehydrated in a graded series of ethanol and embedded in Epon 812. Ultrathin sections were treated with uranyl acetate followed by lead citrate and were examined with an electron microscope (JEM-1200EX, JEOL, Tokyo, Japan).

2.9. Statistical analysis

Comparison of means among three or more groups was done by the Scheffé's method. All results with a p value of less than 0.05 were considered statistically significant.

3. Results

3.1. Mo-DCs support naive CD4$^+$ T cell survival

When naive CD4$^+$ T cells were cultured in RPMI medium in the absence of Mo-DCs, CD4$^+$ T cell numbers decreased daily. Coculture of CD4$^+$ T cells with Mo-DCs at a ratio of 10:1 significantly supported CD4$^+$ T cell survival (Fig. 1A). Mo-DCs supported CD4$^+$ T cell survival in a dose-dependent manner (Fig. 1B). Taken together, CD4$^+$ T cells and Mo-DCs were principally used at a cell ratio of 10:1 throughout this study. To examine whether direct contact between CD4$^+$ T cells and Mo-DCs was required to support CD4$^+$ T cell survival, we used a separated cell-culture system as described in Materials and methods. When CD4$^+$ T cells were cultured without direct contact with Mo-DCs, the number of CD4$^+$ T cells decreased compared to that in mixed cultures but increased significantly compared to that of CD4$^+$ T cells alone (Fig. 2A). Because it is believed that small Mo-DC-derived components that can pass through 0.4-μm filters may have a supportive effect on naive CD4$^+$ T cell survival, we speculated that cytokines such as IL-4, IL-7, or IL-15 may be involved. Culture supernatants were filtered with a filter that allows components smaller than 100 kDa to pass through. Both passed (cytokine-rich) and nonpassed (cytokine-poor) fractions were re-adjusted to the original volume with RPMI medium. Contrary to our expectation, the nonpassed fraction but not the passed fraction supported naive CD4$^+$ T cell survival (Fig. 2B).

We next examined which molecules contribute to the prolonged in vitro survival of naive CD4$^+$ T cells. We focused on MHC class II proteins, particularly HLA-DR, which is expressed on Mo-DCs. Pretreatment of Mo-DCs with anti-HLA-DR mAb inhibited the supportive effect on CD4$^+$ T cell survival (Fig. 3A). Interestingly, addition of anti-HLA-DR mAb to the nonpassed fraction also significantly decreased the number of cells (Fig. 3B).

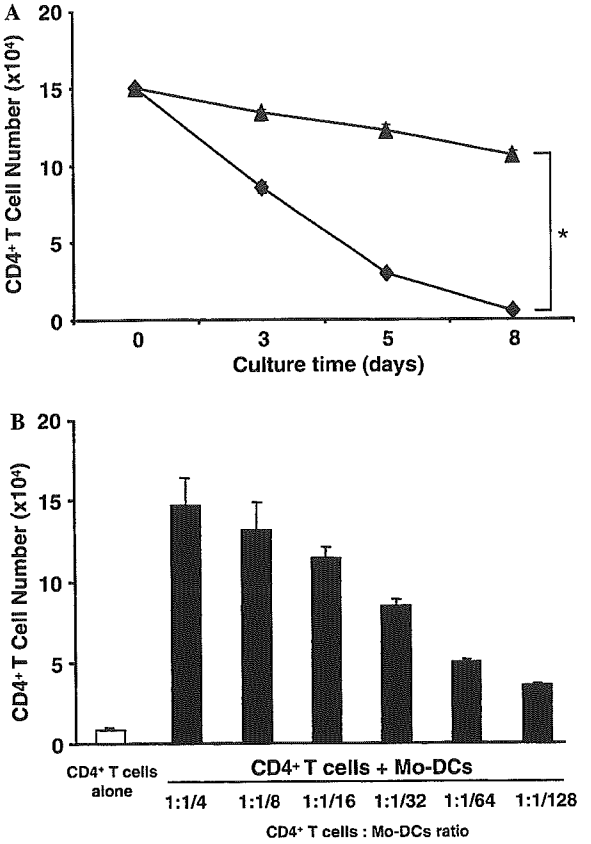

Fig. 1. Coculture with Mo-DCs supports naive CD4$^+$ T cell survival. (A) Purified naive CD4$^+$ T cells were cultured in RPMI medium with (closed triangle) or without (closed diamond) autologous Mo-DCs at a ratio of 10:1. Cell numbers of the viable CD4$^+$ T cells were counted on the indicated days after dead cell exclusion by trypan blue staining. Values represent the means ± SD of triplicate determinations. The asterisk indicates significant differences <0.0001. The data are representative of six independent experiments using Mo-DCs and CD4$^+$ T cells obtained from three different healthy donors. (B) Mo-DCs support naive CD4$^+$ T cell survival in a dose-dependent manner. Purified naive CD4$^+$ T cells (1.5×10^5/150 μl) were cultured with indicated cell numbers of Mo-DCs for 5 days. The data are representative of three independent experiments using Mo-DCs and CD4$^+$ T cells obtained from three different healthy donors.

3.2. Exosomes are present in Mo-DC culture supernatant

We speculated that the HLA-DR-bearing components in the nonpassed fraction may be insoluble substances such as membrane fragments or exosomes. Crude exosomes and purified exosomes were collected from Mo-DC culture supernatants as described in Materials and methods. FACS analysis revealed that 21.5% of the particles in the crude exosomes were positive for both HLA-DR and CD86 (data not shown). The FACS cytogram of purified exosomes coupled to mAb-coated beads showed three populations: single beads, clumps of two beads, and clumps of three or more beads, from the dot-plot representation of forward and side scatter (Fig. 4A-1), as described previously [29]. Single beads represented more

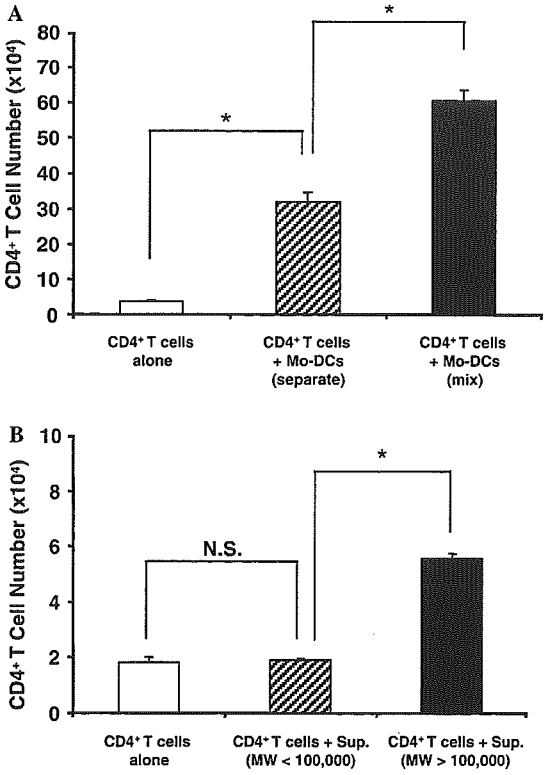

Fig. 2. Supportive effects of Mo-DCs on naive CD4$^+$ T cell survival without direct cellular contact. (A) Viable cell numbers of naive CD4$^+$ T cells cultured in chambers separated by a membrane with pores from Mo-DCs (hatched column) or in the mixture without separation (filled column) were counted on day 5. In only this experiment using separated cell-culture system, CD4$^+$ T cells (1.5×10^6 cells) were cultured with Mo-DCs (1.5×10^5 cells) in 1.5 ml of RPMI medium or were cultured separately in RPMI medium (1.5 ml) with a 0.4-μm separated cell-culture system. Open column shows the cell number of viable naive CD4$^+$ T cells cultured without Mo-DCs. Values represent means ± SD of triplicate determinations. The asterisks indicate significant differences <0.0001. The data are representative of three independent experiments using Mo-DCs and CD4$^+$ T cells obtained from three different healthy donors. (B) Naive CD4$^+$ T cells were cultured in the presence of the culture supernatant of Mo-DCs for 3 days and then the viable cell numbers of the cells were counted. Each column shows the viable cell numbers of the T cells cultured with components smaller than MW 100,000 (hatched column), those larger than MW 100,000 (closed column) or RPMI medium only (open column). Values represent means ± SD of triplicate determinations. The asterisk indicates significant differences 0.0004. N.S. shows not significant. The data are representative of three independent experiments using Mo-DCs and CD4$^+$ T cells obtained from three different healthy donors.

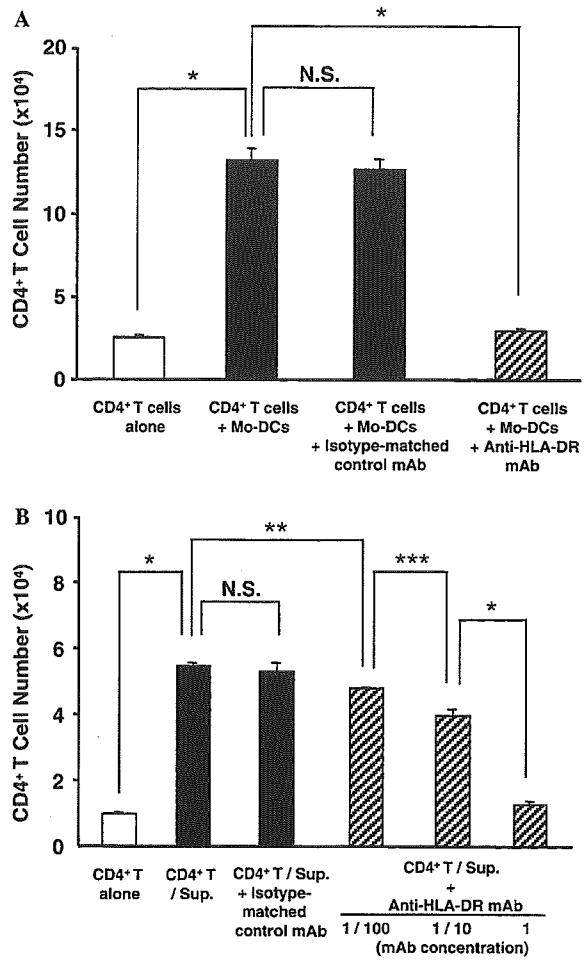

Fig. 3. Requirement of TCR-MHC class II interaction for the prolonged naive CD4$^+$ T cells survival. (A) Viable cell numbers of naive CD4$^+$ T cells cultured with Mo-DCs for 5 days in the presence of anti-MHC class II mAb (4 μg/ml) (hatched column) or isotype-matched control mAb (closed column) were shown. The asterisk indicates significant differences <0.0001. N.S. shows not significant. (B) Naive CD4$^+$ T cells were cultured in the presence of the culture supernatant of Mo-DCs (components of larger than MW 100,000) with anti-MHC class II mAb (hatched column) or with isotype-matched control mAb (closed column) for 4 days and then the viable cell numbers of the cells were counted. The asterisks indicate significant differences <0.0001 (*), 0.002 (**), and 0.007 (***). N.S. shows not significant. Values represent means ± SD of triplicate determinations. The data are representative of three independent experiments using Mo-DCs and CD4$^+$ T cells obtained from three different healthy donors.

than 85% of the total number. The populations containing clumped beads were removed from the analysis by gating for single beads only. More than 90% of the single beads were positive for both HLA-DR and CD86 (Fig. 4A-2). These data indicate that 20% of the particles in the crude exosomes and 90% of the particles in the purified exosomes consist of intact HLA-DR- and CD86-expressing exosomes. Electron microscopic analysis confirmed that the substances coupled to the beads were exosomes (Figs. 4B-1 and B-2). These substances showed the characteristic saucer-like morphology of a flattened sphere limited by a lipid bilayer. The exosomes coupled to the beads ranged from 40 to 140 nm in diameter (means ± SD, 78.46 ± 11.04 nm). The average size of a bead and a CD4$^+$ T cell is 4500 and 7250 nm, respectively.

3.3. Mo-DC-derived exosomes support naive CD4$^+$ T cell survival

To confirm that exosomes are involved in supporting in vitro naive CD4$^+$ T cell survival, purified exosomes

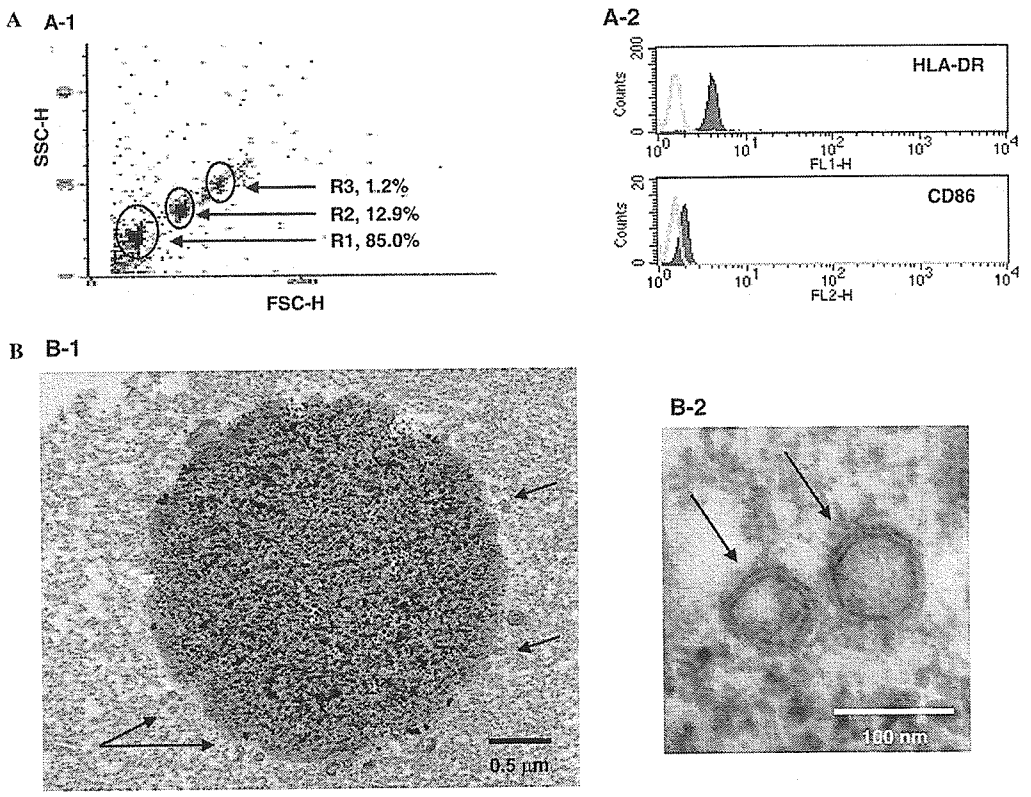

Fig. 4. Detection of MHC class II and CD86 molecules in the components of over MW 100,000 supernatant and electron microscopic characterization of the component. (A) Purified components in supernatants coupled with anti-HLA-DR mAb-coated beads were stained with anti-HLA-DR or anti-CD86 mAbs, and then analyzed by FACS. Three populations of the stained beads appeared in the forward (FSC) and side scatter (SSC) plot are indicated as R1, R2, and R3, respectively and the percentages of each population are also shown (A-1). Histograms show staining of beads for anti-HLA-DR or anti-CD86 (filled line) or control IgG (bold line) on gated R1 area (A-2). The data are representative of three independent experiments. (B) Purified components in supernatants coupled with beads were characterized by electron microscope. Small vesicles (arrows) coating on the surface of the bead (B-1), bar = 0.5 μm and two vesicles of higher magnification (B-2) are shown, bar = 100 nm. The data are representative of six independent experiments using Mo-DCs and $CD4^+$ T cells obtained from three different healthy donors.

coupled to mAb-coated beads were used as effector components. Purified exosomes but not beads alone significantly supported naive $CD4^+$ T cell survival in a dose-dependent manner (Fig. 5A). When beads alone were added to $CD4^+$ T cells, several dying cells were found, and the beads did not bind firmly to any $CD4^+$ T cells. When exosome-coupled beads (purified exosomes) were added to $CD4^+$ T cells, only a few dying cells were found, and the beads bound firmly to several living $CD4^+$ T cells (Fig. 5B). Anti-HLA-DR mAb abrogated the supportive effect of purified exosomes on naive $CD4^+$ T cell survival (Fig. 5C). Anti-HLA-DR mAb also inhibited the binding of exosome-coupled beads to naive $CD4^+$ T cells (data not shown).

3.4. Exosomes induce NF-κB activation in naive $CD4^+$ T cells

We hypothesized that interaction between HLA-DR on exosomes and TCRs on $CD4^+$ T cells induces NF-κB activation, and, as a result, these cells can survive even in severe culture conditions. NF-κB activation of naive $CD4^+$ T cells was estimated by EMSA. Crude exosomes induced NF-κB activation in naive $CD4^+$ T cells within 30 min. Specificity of DNA binding was confirmed by a competition study with a 50-fold excess of unlabeled oligonucleotide. Anti-HLA-DR mAb (4 μg/ml) was added to crude exosomes 1 h prior to coculture with naive $CD4^+$ T cells. Treatment with anti-HLA-DR mAb suppressed exosome-induced NF-κB activation. A NF-κB inhibitor, PDTC (100 μM), was added to naive $CD4^+$ T cells 1 h prior to treatment with crude exosomes. PDTC inhibited nuclear translocation of NF-κB p65 (Fig. 6). PDTC inhibited the supportive effect of crude exosomes on naive $CD4^+$ T cell survival in a dose-dependent manner between 3 and 5 μM without significant direct cytotoxic effect (Fig. 7). These data suggest that exosome-induced NF-κB activation plays a critical role in the survival of naive $CD4^+$ T cells in vitro.

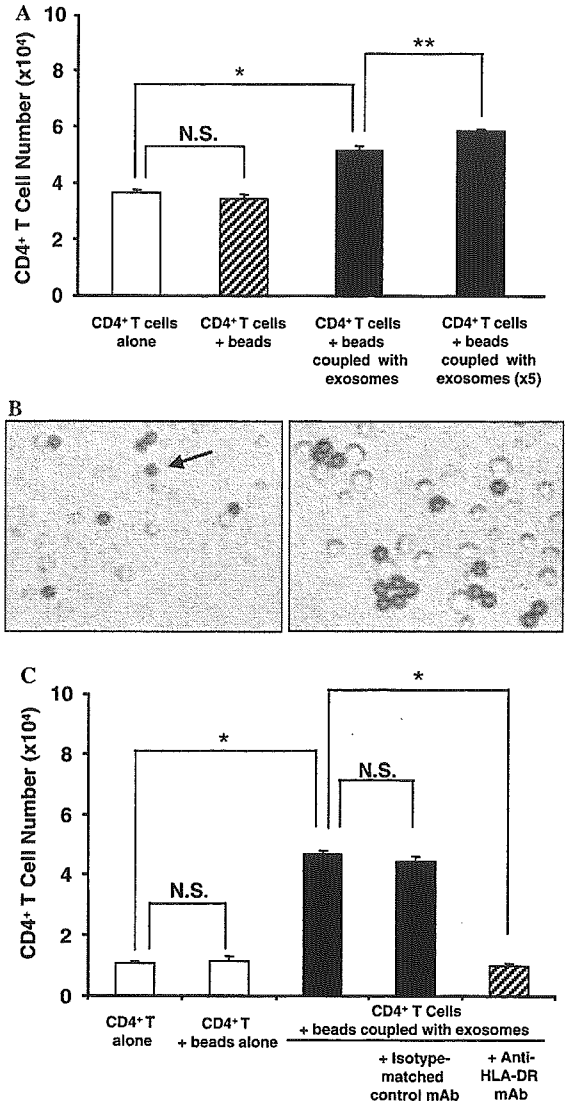

Fig. 5. Prolonged survival of naive $CD4^+$ T cells by interaction with exosomes coupled to anti-MHC class II mAb-coated beads. (A) Viable cell numbers of naive $CD4^+$ T cells cultured with exosomes coupled to anti-MHC class II mAb-coated beads (closed column) for 5 days are shown. Viable cell numbers of $CD4^+$ T cells alone (open column) and $CD4^+$ T cells with anti-HLA-DR mAb-coated beads only (hatched column) are also shown. The asterisk indicates significant differences <0.0001 (*) and 0.0029 (**). N.S. shows not significant. The data are representative of three independent experiments using Mo-DCs and $CD4^+$ T cells obtained from three different healthy donors. (B) Phase-contrast photomicrographs of $CD4^+$ T cells 5 days after coculture with beads (arrow) alone (left panel) and beads coupled with exosomes (right panel). The pictures are representative of three independent experiments using Mo-DCs and $CD4^+$ T cells obtained from three different healthy donors. (C) Viable cell numbers of $CD4^+$ T cells cultured with exosome-coupled beads in the presence (hatched column) or the absence (closed column) of anti-HLA-DR mAb or in the presence (closed column) of isotype-matched control mAb. Open column shows the viable cell number of $CD4^+$ T cells alone and $CD4^+$ T cells cultured with beads alone. The asterisk indicates significant differences <0.0001. N.S. shows not significant. Values represent means ± SD of triplicate determinations. The data are representative of three independent experiments using Mo-DCs and $CD4^+$ T cells obtained from three different healthy donors.

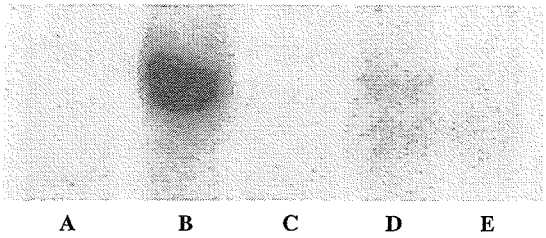

Fig. 6. NF-κB activation in naive $CD4^+$ T cells induced by crude exosomes. The nuclear translocation of NF-κB p65 of naive $CD4^+$ T cells in response to exosomes was determined by EMSA. Naive $CD4^+$ T cells were incubated for 30 min for various conditions as below. Lane A, medium only; lane B, crude exosomes; lane C, crude exosomes with NF-κB ODN (50×); lane D, crude exosomes with anti-HLA-DR mAb; and lane E, crude exosomes with PDTC (100 μM). The data are representative of three independent experiments using Mo-DCs and $CD4^+$ T cells obtained from three different healthy donors.

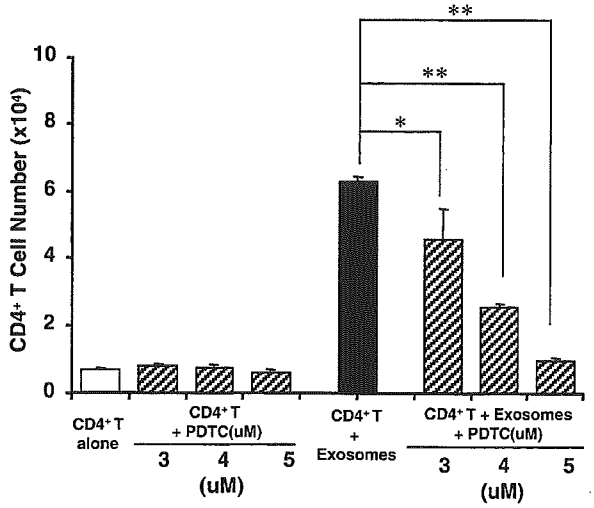

Fig. 7. Suppression of exosome-induced prolonged survival of naive $CD4^+$ T cells by NF-κB inhibitor PDTC. Viable cell numbers of naive $CD4^+$ T cells cultured with crude exosomes (closed column), crude exosomes with indicated concentrations of PDTC (hatched column) or medium alone (open column) for 5 days are shown. The asterisks indicate significant differences 0.0016 (*), <0.0001 (**). Values represent means ± SD of triplicate determinations. The data are representative of three independent experiments using Mo-DCs and $CD4^+$ T cells obtained from three different healthy donors.

4. Discussion

We showed that Mo-DC-derived exosomes can prolong naive $CD4^+$ T cell survival in an HLA-DR-dependent manner. Our data also suggest that NF-κB activation induced by exosomes contributes to this increased survival.

Several players such as TCRs and CD28 are related to T cell survival [5,30]. In the last two decades, many in vivo studies in mice have shown that long-term survival of naive $CD4^+$ T cells requires interaction with self-MHC class II proteins [1–3]. However, it remains

unclear whether interaction with these proteins can prolong the short-term survival of naive $CD4^+$ T cells in vitro. Recently, it was shown that human Mo-DCs expressing abundant MHC class II proteins are able to support short-term survival of T cells in vitro [7]. Interestingly, our present findings indicate that although HLA-DR is critical for naive $CD4^+$ T cell survival in vitro (Fig. 3A), direct interaction between Mo-DCs and T cells is not always required (Fig. 2A). It has been shown that MHC class II proteins are very abundant in exosomes from APCs [10]. In the present study, Mo-DCs also released exosomes into culture medium, and Mo-DC-derived exosomes expressed both MHC class II and CD86 proteins (Fig. 4A). Recently, it was reported that MHC class II proteins on released exosomes are functional [10,31]. Raposo et al. [10] showed that exosomes derived from both human and murine B lymphocytes induce antigen-specific MHC class II-restricted T cell responses. Vincent-Schneider et al. [31] showed that the combination of exosomes with DCs results in highly efficient stimulation of specific T cells and suggested that exosome-bearing MHC class II complexes are taken up by dedicated APCs for efficient T cell activation. On the basis of these findings, we hypothesized that Mo-DC-derived exosomes can prolong naive $CD4^+$ T cell survival. To prove this, we used exosomes purified with human anti-HLA-DP, -DQ, or -DR-coated paramagnetic beads. To avoid contamination with serum-derived exosomes [32], we used RPMI 1640 medium supplemented with 1% human albumin. Purified exosomes prolonged naive $CD4^+$ T cell survival in an HLA-DR-dependent manner (Fig. 5C).

The present study shows a novel function of exosomes. Mo-DC-derived exosomes express not only MHC class II but also CD86 proteins. CD28, which is a ligand for CD86, is believed to contribute to T cell survival [29]. In our study, peripheral monocytes, in which CD86 expression is weak, did not prolong $CD4^+$ T cell survival (data not shown), suggesting a possible role of a CD28/CD86 interaction. But our data that specific antibody against HLA-DR inhibited completely the effect of exosomes on $CD4^+$ T cell survival. These data indicate that TCR is a likely candidate for transmitting the viability signal. However, participation of other receptors for MHC class II such as LAG-3 has not been excluded [33]. Furthermore, other molecular events, such as CD28/CD86 interaction, in addition to the interaction between TCR and HLA-DR may operate in prolongation of $CD4^+$ T cell survival induced with exosomes. A role of exosome-bearing CD86 in $CD4^+$ T cell survival has not been reported, and the mechanism of exosome-induced, HLA-DR-dependent naive $CD4^+$ T cell survival is not clear. Several transcription factors such as Ets, NFAT, AP-1, and NF-κB have been shown to be activated by TCRs or CD28 [20]. Recent studies have indicated that NF-κB plays a key role in T cell survival. For example, it has been suggested that the PI3K/Akt pathway is important for the effects of both CD28 and IL-2R [23,34,35], and NF-κB is thought to be target of Akt [36,37]. More direct evidence that NF-κB contributes to T cell survival has been reported recently [22,26]. In p50−/− cRel−/− mice, which exhibit virtually no inducible κB site binding activity, an essential role of TCR-induced NF-κB was indicated in T cell survival [26]. In addition, NF-κB regulated TCR-induced expression of anti-apoptotic Bcl-2 family members and NF-κB activation was not only necessary but was also sufficient for T cell survival [38]. Wan and DeGregon [22] reported that the survival of antigen-stimulated T cells requires NF-κB-mediated inhibition of p73 expression. Our present data show for the first time that Mo-DC-derived exosomes can induce NF-κB activation in naive $CD4^+$ T cells (Fig. 6). PDTC is a stable analog of dithiocarbamate and is one of the most widely used inhibitors of NF-κB signaling [39]. Although it has been postulated that PDTC acts simply as an antioxidant to inhibit NF-κB activation [40], it has been shown definitively that PDTC inhibits NF-κB activation independently of antioxidative function [41]. In the present study, we used PDTC to examine contribution of the NF-κB pathway to exosome-mediated $CD4^+$ T cell survival. PDTC inhibited the supportive effect of exosomes on $CD4^+$ T cell survival in a dose-dependent manner without significant direct cytotoxic effect (Fig. 7). These results suggest that NF-κB plays an essential role in exosome-mediated $CD4^+$ T cell survival. However, we have no definitive evidence as to how exosomes induce NF-κB in naive $CD4^+$ T cells.

It has been reported that DC-derived exosomes may be used as vectors for vaccination because they express high levels of functional MHC class I– and class II–peptide complexes, together with CD86 [10,14,19]. A recent report showed that MHC class I proteins on purified exosomes from DCs can be directly loaded with peptide at much greater levels than by indirect loading [17]. Also reported was a new exosome purification procedure from Mo-DCs [14], in which ultrafiltration through a 500-kDa membrane and ultracentrifugation into a 30% sucrose/deuterium-oxide cushion made it possible to recover up to 50% exosomes. Although the function of most of the exosome-bearing proteins is unknown at present, accumulated data on exosome function suggest that these proteins will become exciting therapeutic tools in the near future.

Acknowledgments

We thank Yasuhiro Hirakawa (Department of Anatomy and Cell Biology affiliation), Takaaki Kanemaru, and Kaori Nomiyama for technical assistance.

References

[1] S. Takeda, H.R. Rodewald, H. Arakawa, H. Bluethmann, T. Shimizu, MHC class II molecules are not required for survival of newly generated CD4+ T cells, but affect their long-term life span, Immunity 5 (1996) 217–228.

[2] T. Brocker, Survival of mature CD4 T lymphocytes is dependent on major histocompatibility complex class II-expressing dendritic cells, J. Exp. Med. 186 (1997) 1223–1232.

[3] S. Garcia, J. DiSanto, B. Stockinger, Following the development of a CD4 T cell response in vivo: from activation to memory formation, Immunity 1 (1999) 163–171.

[4] C. Tanchot, F.A. Lemonnier, B. Perarnau, A.A. Freitas, B. Rocha, Differential requirements for survival and proliferation of CD8 naive or memory T cells, Science 276 (1997) 2057–2062.

[5] J. Kirberg, A. Berns, H. von Boehmer, Peripheral T cell survival requires continual ligation of the T cell receptor to major histocompatibility complex-encoded molecules, J. Exp. Med. 186 (1997) 1269–1275.

[6] C. Viret, F.S. Wong, C.A. Janeway Jr., Designing and maintaining the mature TCR repertoire: the continuum of self-peptide:self-MHC complex recognition, Immunity 10 (1999) 559–568.

[7] T. Kondo, I. Cortese, S. Markovic-Plese, K.P. Wandinger, C. Carter, M. Brown, S. Leitman, R. Martin, Dendritic cells signal T cells in the absence of exogenous antigen, Nat. Immunol. 2 (2001) 932–938.

[8] E.G. Trams, C.J. Lauter, N. Salem Jr., U. Heine, Exfoliation of membrane ecto-enzymes in the form of micro-vesicles, Biochim. Biophys. Acta 645 (1981) 63–70.

[9] R.M. Johnstone, M. Adam, J.R. Hammond, L. Orr, C. Turbide, Vesicle formation during reticulocyte maturation. Association of plasma membrane activities with released vesicles (exosomes), J. Biol. Chem. 262 (1987) 9412–9420.

[10] G. Raposo, H.W. Nijman, W. Stoorvogel, R. Liejendekker, C.V. Harding, C.J. Melief, H.J. Geuze, B lymphocytes secrete antigen-presenting vesicles, J. Exp. Med. 183 (1996) 1161–1172.

[11] J.Q. Davis, D. Dansereau, R.M. Johnstone, V. Bennett, Selective externalization of an ATP-binding protein structurally related to the clathrin-uncoating ATPase/heat shock protein in vesicles containing terminal transferrin receptors during reticulocyte maturation, J. Biol. Chem. 261 (1986) 15368–15371.

[12] C. Thery, M. Boussac, P. Veron, P. Ricciardi-Castagnoli, G. Raposo, J. Garin, S. Amigorena, Proteomic analysis of dendritic cell-derived exosomes: a secreted subcellular compartment distinct from apoptotic vesicles, J. Immunol. 166 (2001) 7309–7318.

[13] F. Sallusto, A. Lanzavecchia, Efficient presentation of soluble antigen by cultured human dendritic cells is maintained by granulocyte/macrophage colony-stimulating factor plus interleukin 4 and downregulated by tumor necrosis factor alpha, J. Exp. Med. 179 (1994) 1109–1118.

[14] L. Zitvogel, A. Regnault, A. Lozier, J. Wolfers, C. Flament, D. Tenza, P. Ricciardi-Castagnoli, G. Raposo, S. Amigorena, Eradication of established murine tumors using a novel cell-free vaccine: dendritic cell-derived exosomes, Nat. Med. 4 (1998) 594–600.

[15] H.G. Lamparski, A. Metha-Damani, J.Y. Yao, S. Patel, D.H. Hsu, C. Ruegg, J.B. Le Pecq, Production and characterization of clinical grade exosomes derived from dendritic cells, J. Immunol. Methods 270 (2002) 211–226.

[16] C. Thery, L. Duban, E. Segura, P. Veron, O. Lantz, S. Amigorena, Indirect activation of naive CD4+ T cells by dendritic cell-derived exosomes, Nat. Immunol. 3 (2002) 1156–1162.

[17] D.H. Hsu, P. Paz, G. Villaflor, A. Rivas, A. Mehta-Damani, E. Angevin, L. Zitvogel, J.B. Le Pecq, Exosomes as a tumor vaccine: enhancing potency through direct loading of antigenic peptides, J. Immunother. 26 (2003) 440–450.

[18] I. Hwang, X. Shen, J. Sprent, Direct stimulation of naive T cells by membrane vesicles from antigen-presenting cells: distinct roles for CD54 and B7 molecules, Proc. Natl. Acad. Sci. USA 100 (2003) 6670–6675.

[19] D. Skokos, H.G. Botros, C. Demeure, J. Morin, R. Peronet, G. Birkenmeier, S. Boudaly, S. Mecheri, Mast cell-derived exosomes induce phenotypic and functional maturation of dendritic cells and elicit specific immune responses in vivo, J. Immunol. 170 (2003) 3037–3045.

[20] C.T. Kou, J.M. Leiden, Transcriptional regulation of T lymphocyte development and function, Annu. Rev. Immunol. 17 (1999) 149–187.

[21] E. Dudley, F. Hornung, L. Zheng, D. Scherer, D. Ballard, M. Lenardo, NF-kappaB regulates Fas/APO-1/CD95- and TCR-mediated apoptosis of T lymphocytes, Eur. J. Immunol. 29 (1999) 878–886.

[22] Y.Y. Wan, J. DeGregon, The survival of antigen-stimulated T cells requires NFkappaB-mediated inhibition of p73 expression, Immunity 18 (2003) 331–342.

[23] R.G. Jones, M. Parsons, M. Bonnard, V.S. Chan, W.C. Yeh, J.R. Woodgett, P.S. Ohashi, Protein kinase B regulates T lymphocyte survival, nuclear factor kappaB activation, and Bcl-X(L) levels in vivo, J. Exp. Med. 191 (2000) 1721–1734.

[24] S. Ghosh, M.J. May, E.B. Kopp, NF-kB and Rel proteins: evolutionarily conserved mediators of immune responses, Annu. Rev. Immunol. 16 (1998) 225–260.

[25] J.A. DiDonato, F. Mercurio, M. Karin, Phosphorylation of IkB precedes but is not sufficient for its dissociation from NF-kB, Mol. Cell. Biol. 15 (1995) 1302–1311.

[26] Y. Zheng, M. Vig, J. Lyons, L. Van Parijs, A.A. Bed, Combined deficiency of p50 and cRel in CD4+ T cells reveals an essential requirement for nuclear factor kappa B in regulating mature T cell survival and in vivo function, J. Exp. Med. 197 (2003) 861–874.

[27] M. Kojima, T. Morisaki, K. Izuhara, A. Uchiyama, Y. Matsunari, M. Katano, M. Tanaka, Lipopolysaccharide increase cyclooxygenase-2 expression in a colon carcinoma cell line through nuclear factor-kappa B activation, Oncogene 19 (2000) 1225–1231.

[28] J.A. Hobot, E. Carlemalm, W. Villiger, E. Kellenberger, Periplasmic gel: new concept resulting from the reinvestigation of bacterial cell envelope ultrastructure by new methods, J. Bacteriol. 160 (1984) 143–152.

[29] A. Clayton, J. Court, H. Navabi, M. Adams, M.D. Mason, J.A. Hobot, G.R. Newman, B. Jasani, Analysis of antigen presenting cell derived exosomes, based on immuno-magnetic isolation and flow cytometry, J. Immunol. Methods 247 (2001) 163–174.

[30] L.H. Boise, A.J. Minn, P.J. Noel, C.H. June, M.A. Accavitti, T. Lindsten, C.B. Thompson, CD28 costimulation can promote T cell survival by enhancing the expression of Bcl-XL, Immunity 3 (1995) 87–98.

[31] H. Vincent-Schneider, P. Stumptner-Cuvelette, D. Lankar, S. Pain, G. Raposo, P. Benaroch, C. Bonnerot, Exosomes bearing HLA-DR1 molecules need dendritic cells to efficiently stimulate specific T cells, Int. Immunol. 14 (2002) 713–722.

[32] G. van Niel, G. Raposo, C. Candalh, M. Boussac, R. Hershberg, N. Cerf-Bensussan, M. Heyman, Intestinal epithelial cells secrete exosome-like vesicles, Gastroenterology 121 (2001) 337–349.

[33] C.J. Workman, D.A. Vignali, The CD4-related molecule, LAG-3 (CD223), regulates the expansion of activated T cells, Eur. J. Immunol. 33 (2003) 970–979.

[34] J.S. Burr, N.D. Savage, G.E. Messah, S.L. Kimzey, A.S. Shaw, R.H. Arch, J.M. Green, Cutting edge: distinct motifs within CD28 regulate T cell proliferation and induction of Bcl-XL, J. Immunol. 166 (2001) 5331–5335.

[35] K.A. Frauwirth, J.L. Riely, M.H. Harris, R.V. Parry, J.C. Rathmell, D.R. Plas, R.L. Elstrom, C.H. June, C.B. Thompson, The CD28 signaling pathway regulates glucose metabolism, Immunity 16 (2002) 769–777.

[36] L.P. Kane, V.S. Shapiro, D. Stokoe, A. Weiss, Induction of NF-kappaB by the Akt/PKB kinase, Curr. Biol. 9 (1999) 601–604.
[37] J.A. Romashkova, S.S. Makarov, NF-kappaB is a target of AKT in anti-apoptotic PDGF signaling, Nature 401 (1999) 86–90.
[38] R.J. Grumont, I.J. Rourke, S. Gerondakis, Rel-dependent induction of A1 transcription is required to protect B cells from antigen receptor ligation-induced apoptosis, Genes Dev. 13 (1999) 400–411.
[39] P.A. Baeuerle, T. Henkel, Function and activation of NF-kB in the immune system, Annu. Rev. Immunol. 12 (1994) 141–179.
[40] L. Flohe, R. Brigelius-Flohe, C. Saliou, M.G. Traber, L. Packer, Redox regulation of NF-kappa B activation, Free Radic. Biol. Med. 22 (1997) 1115–1126.
[41] M. Hayakawa, H. Miyashita, I. Sakamoto, M. Kitagawa, H. Tanaka, H. Yasuda, M. Karin, K. Kikugawa, Evidence that reactive oxygen species do not mediate NF-kB activation, EMBO J. 22 (2003) 3356–3366.

DNA vaccination of HSP105 leads to tumor rejection of colorectal cancer and melanoma in mice through activation of both CD4+ T cells and CD8+ T cells

Masafumi Miyazaki,[1,2,6] Tetsuya Nakatsura,[1,6] Kazunori Yokomine,[1] Satoru Senju,[1] Mikio Monji,[1] Seiji Hosaka,[1] Hiroyuki Komori,[1,2] Yoshihiro Yoshitake,[1] Yutaka Motomura,[1,2] Motozumi Minohara,[4] Tatsuko Kubo,[3] Keiichi Ishihara,[5] Takumi Hatayama,[5] Michio Ogawa[2] and Yasuharu Nishimura[1,6]

[1]Department of Immunogenetics, [2]Department of Surgery II, and [3]Department of Molecular Pathology, Graduate School of Medical Sciences, Kumamoto University, 1-1-1 Hongo, Kumamoto 860–8556; [4]Department of Neurology, Neurological Institute, Graduate School of Medical Sciences, Kyushu University, 3-1-1 Maidashi, Higashi-ku, Fukuoka 812-8582; and [5]Department of Biochemistry, Kyoto Pharmaceutical University, 5 Nakauchi-cho, Misasagi, Yamashina-ku, Kyoto 607-8414, Japan

(Received May 25, 2005/Revised July 7, 2005/Accepted July 11, 2005/Online publication August 29, 2005)

We report that HSP105, identified by serological identification of antigens by recombinant expression cloning (SEREX), is overexpressed in a variety of human cancers, including colorectal, pancreatic, thyroid, esophageal, and breast carcinoma, but is not expressed in normal tissues except for the testis. The amino acid sequences and expression patterns of HSP105 are very similar in humans and mice. In this study, we set up a preclinical study to investigate the usefulness of a DNA vaccine producing mouse HSP105 whole protein for cancer immunotherapy *in vivo* using BALB/c and C57BL/6 mice, Colon26, a syngeneic endogenously HSP105-expressing colorectal cancer cell line, and B16.F10, a melanoma cell line. The DNA vaccine was used to stimulate HSP105-specific T-cell responses. Fifty percent of mice immunized with the *HSP105* DNA vaccine completely suppressed the growth of subcutaneous Colon26 or B16.F10 cells accompanied by massive infiltration of both CD4+ T cells and CD8+ T cells into tumors. In cell transfer or depletion experiments we proved that both CD4+ T cells and CD8+ T cells induced by these vaccines play critical roles in the activation of antitumor immunity. Evidence of autoimmune reactions was not present in surviving mice that had rejected tumor cell challenges. We found that HSP105 was highly immunogenic in mice and that the *HSP105* DNA vaccination induced antitumor immunity without causing autoimmunity. Therefore, HSP105 is an ideal tumor antigen that could be useful for immunotherapy or the prevention of various human tumors that overexpress HSP105, including colorectal cancer and melanoma. (*Cancer Sci* 2005; 96: 695–705)

Colorectal cancer (CRC) and melanoma are common and serious malignancies, for which surgery remains the main treatment, although the success of the treatment depends on the stage of the disease. Although adjuvant systemic chemotherapy or chemoradiation can confer a limited but significant survival advantage, novel and more effective therapies are needed. Identification of tumor associated antigens (TAA) expressed by CRC or melanomas remains one of the goals for designing novel immunological treatments for these tumors. Ideal targets for immunotherapy are gene products that are silenced in normal tissues except immune privilege tissue such as testis tissue, and that are overexpressed in cancer cells.

More than 2000 candidate TAA have been identified by using the serological identification of antigens by recombinant expression cloning (SEREX) method. We have also reported TAA identified by using this method.[1–4] We earlier found that HSP105 (often called HSP110), as identified by SEREX was overexpressed specifically in a variety of human cancers, including colorectal, pancreatic, thyroid, esophageal, and breast carcinoma, but was not expressed in normal tissues except for testis tissue.[1,5] We recently found that HSP105 was also overexpressed in melanoma (unpublished data). If HSP105 can induce strong antitumor immunity, it may be a potential candidate as a target antigen for cancer immunotherapy. In the present study, we set up a preclinical study to investigate the usefulness of a *HSP105*-DNA vaccine, using BALB/c and C57BL/6 mice, the syngeneic endogenously HSP105-expressing CRC cell line Colon26, and the melanoma cell line B16.F10. Using these models, we analyzed both the antitumor effects and side-effects, including autoimmunity of the *HSP105* DNA vaccination.

The pioneering studies of Srivastava and colleagues led to the proposal that several HSP, including HSP70, HSP90 and gp96, bind antigenic peptides and deliver these peptides (through receptor-mediated endocytosis of the HSP) into the antigen-processing pathway of the antigen presenting cell (APC) for presentation on major histocompatibility complex (MHC) class I molecules. This HSP-involved pathway has been demonstrated to evoke potent antiviral and antitumor immune responses.[6] However, many researchers have identified MHC class I-presented peptide epitopes derived from HSP. HSP are

M. Miyazaki and T. Nakatsura contributed equally to this work.

[6]To whom correspondence should be addressed. E-mail: mxnishim@gpo.kumamoto-u.ac.jp or tnakatsu@kaiju.medic.kumamoto-u.ac.jp

Abbreviations: C26 (C20), Colon26 clone 20; CRC, colorectal cancer; CTL, cytotoxic T lymphocytes; HE, hematoxylin and eosin; HSP105, heat shock protein 105; APC, antigen presenting cell; mAb, monoclonal antibody; MHC, major histocompatibility complex; SEREX, serological identification of antigens by recombinant expression cloning; TAA, tumor associated antigens.

 doi: 10.1111/j.1349-7006.2005.00093.x

rich sources of MHC-bound peptides, and the expression of these peptides increases as a result of cellular stresses.[7]

Recently, Subjeck and colleagues tested a vaccine using the chaperoning properties of HSP110 as Srivastava and colleagues had done before them.[8,9] They reported that HSP110 overexpression increases the immunogenicity of murine CT26 colon tumors.[10] *HSP110* cloned from CHO cells[11] and *HSP105* cloned from mice[12] and humans[13] are homologs. We show here that this HSP105 is highly immunogenic for stimulating tumor immunity against mouse CRC and melanoma. Furthermore, both $CD4^+$ T cells and $CD8^+$ T cells induced by the *HSP105* DNA vaccination play critical roles in the activation of antitumor immunity. These findings indicate that HSP105 itself could be considered a valuable TAA for the immune-based therapy of various tumors overexpressing HSP105, including CRC and melanoma.

Materials and Methods

Cell lines and mice

A subline of the BALB/c-derived CRC cell line Colon26, C26 (C20),[14] was provided by Dr Kyoichi Shimomura (Fujisawa Pharmaceutical Co., Japan). B16.F10 was kindly provided by the Cell Resource Center for Biomedical Research, Institute of Development, Aging, and Cancer, Tohoku University (Sendai, Japan). These cell lines were maintained *in vitro* in RPMI-1640 medium supplemented with 10% fetal calf serum at 37°C in a 5% CO_2 atmosphere. Female 7-week-old BALB/c mice ($H\text{-}2^d$) and C57BL/6 mice ($H\text{-}2^b$), purchased from Charles River Japan (Yokohama, Japan), were kept in the Center for Animal Resources and Development (CARD) of Kumamoto University, and handled in accordance with the animal care policy of Kumamoto University.

Histological and immunohistochemical analysis

Immunohistochemical detections of HSP105, CD8 and CD4 were carried out as described elsewhere.[1,5,15–18] The primary antibody used in this study, rabbit polyclonal antihuman HSP105 was purchased from Santa Cruz (Santa Cruz, CA, USA). Hematoxylin and eosin (HE) staining and standard methods were used for histological analysis. We purchased Human Normal Organs and Cancer Multi Tissue Slide, BC4, from SuperBioChips Laboratories (Seoul, Korea) for immunohistochemical analysis.

Construction of a mouse *HSP105* expression plasmid DNA

Plasmid pcDNA105, which expresses mouse *HSP105* whole protein was generated as described elsewhere.[12] To construct this plasmid, the mouse *HSP105* full-length cDNA derived from the pB105-1 plasmid was subcloned into *Eco*RV–*Xba*I sites of the mammalian expression vector pcDNA3 (Invitrogen, Osaka, Japan). The pCAGGS expression vector was kindly provided by Dr Junichi Miyazaki (Osaka University, Japan) and this vector induces strong gene expression when injected into muscle.[19] We constructed a pCAGGS-*HSP105* plasmid by inserting mouse *HSP105* cDNA into the *Eco*RI site of the pCAGGS expression vector, which carries the CAG (cytomegalovirus immediate-early enhancer/chicken β-actin hybrid) promoter, and prepared the plasmid using a Qiagen EndoFree plasmid Mega kit (Qiagen GmbH, Hilden, Germany). We used the empty pCAGGS plasmid as a control.

DNA vaccination

We immunized mice twice by intramuscular injection into the anterior tibialis muscle. Booster immunization was carried out at 7 days after the primer immunization. The groups of mice were given the following vaccines: (i) saline group: given with 100 μL saline; (ii) control vector group: given 50 μg pCAGGS plasmids lacking inserts and diluted in 100 μL saline; (iii) *HSP105* DNA vaccine group: given 50 μg of pCAGGS-*HSP105* plasmid diluted in 100 μL saline.

In vivo tumor challenge

Subcutaneous tumors were established by the injection of 3×10^4 C26 (C20) cells or 1×10^4 B16.F10 cells suspended in 100 μL Hanks' Balanced Salt Solution (Gibco, Grand Island, NY, USA) medium into the right flank of BALB/c or C57BL/6 mice 7 days after the last vaccination. Tumor incidence and volume were assessed twice weekly using calipers until the mice died. Tumor area was calculated as a product of width and length. The results are presented as mean area of tumor ± SE; however, individual tumor area is presented for some experiments.

In vivo depletion of $CD4^+$ T cells and $CD8^+$ T cells

Each mouse was given a total of six intraperitoneal transfers (days −18, −15, −11, −8, −4, −1) of ascites (0.1 mL per mouse per transfer) from hybridoma-bearing nude mice. The mAbs used were rat antimouse CD4 (clone GK1.5) and rat antimouse CD8 (clone 2.43). Normal rat IgG (Sigma, St. Louis, MO, USA; 200 μg per mouse per transfer) was used as a control. The depletion of T cell subsets by treatment with mAbs was confirmed by flow cytometric analysis of spleen cells, which showed a > 90% specific depletion.

Cell transfer *in vivo*

We purified $CD8^+$ T cells, $CD4^+$ T cells, and natural killer (NK) cells from spleen cells using the magnetic cell sorting system with antimouse CD8α (Ly-2) mAb, antimouse CD4 (L3T4) mAb, antimouse NK (DX5) mAb, and these $CD8^+$ T cells, $CD4^+$ T cells, and NK cells were used for adoptive transfer into BALB/c mice. To investigate tumor growth in a homeostatic lymphocyte proliferation model, we intravenously injected 1.5×10^7 whole spleen cells or 3×10^6 $CD8^+$ T cells, $CD4^+$ T cells, NK cells, or $CD8^-$ $CD4^-$ NK^- cells 3 days after sublethal irradiation (5 Gy). Subsequently, we subcutaneously inoculated BALB/c mice with C26 cells (3×10^4) 3 days after irradiated mice inoculated with cells.

Statistical analysis

We analyzed all data using the StatView statistical program for Macintosh (SAS, Cary, NC, USA) and evaluated statistical significance using the unpaired *t*-test. The overall survival rate was calculated using the Kaplan–Meier method, and statistical significance was evaluated using Wilcoxon's test.

Results

Similar tissue and cancer-specific expression of HSP105 in mice and humans

We have previously reported that HSP105 is overexpressed in a variety of human cancers, including colorectal, pancreatic, esophageal, thyroid, and breast cancer, whereas HSP105 is

 doi: 10.1111/j.1349-7006.2005.00093.x

expressed at low levels in many normal tissues, except for testis tissue.[1,5] In the present study, we carried out an immunohistochemical analysis of HSP105 using various human and mouse tissues (Fig. 1). Human HSP105 is overexpressed in almost all CRC cells, melanoma cells (unpublished data), and normal testis tissue, but there is no expression or only a low-level expression of HSP105 in normal liver, brain, spleen, lung, and kidney tissue (Fig. 1a). Mouse HSP105 is also overexpressed in liver metastasis of the murine colorectal adenocarcinoma cell line C26 (C20), lung metastasis of the murine melanoma cell line B16.F10 and normal testis tissue, but there is no expression or only low-level expression in normal liver, cerebrum, cerebellum, spleen, lung, and kidney tissue (Fig. 1b). Another group reported that HSP105/110 is expressed in neurons in the cerebrum and Purkinje cells in the cerebellum,[20] we found the same pattern in the present study, but the level of expression in the neurons and Purkinje cells was much weaker than that in CRC and testis tissue (Fig. 1a,b). As a result, the expression levels of HSP105 protein in human colorectal, pancreatic, esophageal, thyroid, and breast cancers, melanoma, C26 tumors, and B16.F10 tumors were evidently much higher than those in all normal adult tissues, including brain, but not testis in both humans and mice. Because the expression pattern of HSP105 is very similar in humans and mice, we are able to analyze both the antitumor effects and side-effects (including autoimmunity) of HSP105 vaccination using this mouse model of CRC and melanoma.

HSP105 DNA induced rejection of C26 and B16.F10 tumor challenge in mice

We investigated the effects of *HSP105* DNA vaccination using a subcutaneously injected C26 (Fig. 2a–d) and B16.F10 (Fig. 2e–h) tumor model. Mice were divided into three groups: mice inoculated with (i) saline; (ii) pCAGGS, and (iii) pCAGGS-*HSP105*. No mice died during the vaccination period.

Subcutaneous inoculation of C26 cells (3×10^4) into the right flank was given 7 days after the last vaccination (Fig. 2a–d). In groups (i) and (ii), subcutaneous tumors appeared in some mice 10 days after inoculation. Measurement of tumor size was continued until 24 days after inoculation with the tumor cells, when one mouse died. The mean tumor size on day 24 in group (iii) mice (26.4 ± 10.8 mm^2) was significantly smaller than that in the other two groups (105.0 ± 15.7, and 86.0 ± 8.3 mm^2, respectively; $P < 0.05$; Fig. 2a). Six of the 10 mice (60%) in group (iii) did not have subcutaneous tumors on day 24 (Fig. 2b). All mice in groups (i) and (ii) had subcutaneous tumors within 13 days, and died within 41 days of inoculation with the tumor cells (Fig. 2c,d). Five of the 10 mice (50%) in group (iii) completely rejected the 3×10^4 C26 cells during the 108 days after the inoculation (Fig. 2c,d). A statistically significant difference in survival time was found between group (iii) and groups (i) and (ii) ($P < 0.05$).

Subcutaneous inoculation of B16.F10 cells (1×10^4) into the right flank was carried out 7 days after the last vaccination (Fig. 2e–h). Measurement of tumor size was continued until 30 days after inoculation with the tumor cells, when one mouse died. Mean tumor size on day 30 in group (iii) mice (103.9 ± 49.8 mm^2) was significantly smaller than that in the other two groups (272.1 ± 69.7, and 361.6 ± 50.3 mm^2, respectively; $P < 0.05$; Fig. 2e). Six of eight mice (75%) in group (iii) did not have subcutaneous tumors on day 30 (Fig. 2f). All mice in groups (i) and (ii) had subcutaneous tumors within 41 days, and died within 65 days of inoculation with the tumor cells (Fig. 2g,h). Four of eight mice (50%) in group (iii) completely rejected the 1×10^4 B16.F10 cells during the 100 days after the inoculation (Fig. 2g,h). A statistically significant difference in survival time was found between group (iii) and groups (i) and (ii) ($P < 0.05$). Therefore, the *HSP105* DNA vaccine has the potential to prevent the growth of tumors expressing HSP105.

We also subcutaneously inoculated five surviving group (iii) mice that completely rejected the first challenges with C26 cells with further (3×10^4) C26 cells. These mice also rejected the second challenge with C26 cells, even at 108 days after the first challenge (data not shown). These results demonstrate that the effects of vaccination in group (iii) continued for a long time, and that the vaccination prevented the recurrence of HSP105-expressing tumors.

Expression of HSP105 protein and infiltration of CD4$^+$ T cells and CD8$^+$ T cells in the injection sites

To observe HSP105 expression and infiltrating cells in muscles injected with the *HSP105* DNA vaccine, we carried out intramuscular immunizations with pCAGGS DNA into the right anterior tibialis muscle, and with pCAGGS-*HSP105* DNA into the left anterior tibialis muscle of four mice. After 48 h, we killed the mice and evaluated the muscles by histological and immunohistochemical analysis (Fig. 3). In HE-stained sections, there were some transverse sections of injection sites that included many cells in both the pCAGGS- and pCAGGS-*HSP105*-immunized muscles. But only in the transverse sections of the injection sites in pCAGGS-*HSP105*-immunized muscles could we observe many cells expressing HSP105 at a high level, and also a considerable number of both CD4$^+$ T cells and CD8$^+$ T cells. Although we did not immunohistochemically stain the dendritic cells in these traverse sections, we did find some dendritic cell-like large cells.

Infiltration of CD4$^+$ T cells and CD8$^+$ T cells into the C26 tumor after vaccination

To observe the antitumor effects of *HSP105 DNA*-vaccination, we evaluated the tumor using immunohistochemical staining of CD8 and CD4. Figure 4a shows the tumor inoculation sites from two *HSP105* DNA-immunized mice, a saline-inoculated mouse, and a pCAGGS-immunized mouse that did not reject the tumor challenge. There were few lymphocytes in the tumors removed from both the saline-inoculated mouse and the pCAGGS immunized mouse, but there were many CD4$^+$ T cells and considerable numbers of CD8$^+$ T cells making contact with the tumor cells and surrounding the tumors removed from the two *HSP105* DNA-immunized mice. These layers of CD4$^+$ T cells surrounding the tumor were thick in the case of *HSP105 DNA* vaccinated mice. Furthermore, there were a considerable number of CD8$^+$ T cells and CD4$^+$ T cells that had infiltrated into the tumor (Fig. 4a).

Vaccination with *HSP105* DNA did not induce damage of normal tissues

HSP105 expression in normal adult mice is limited to several tissues, and HSP105 expression levels in these tissues are

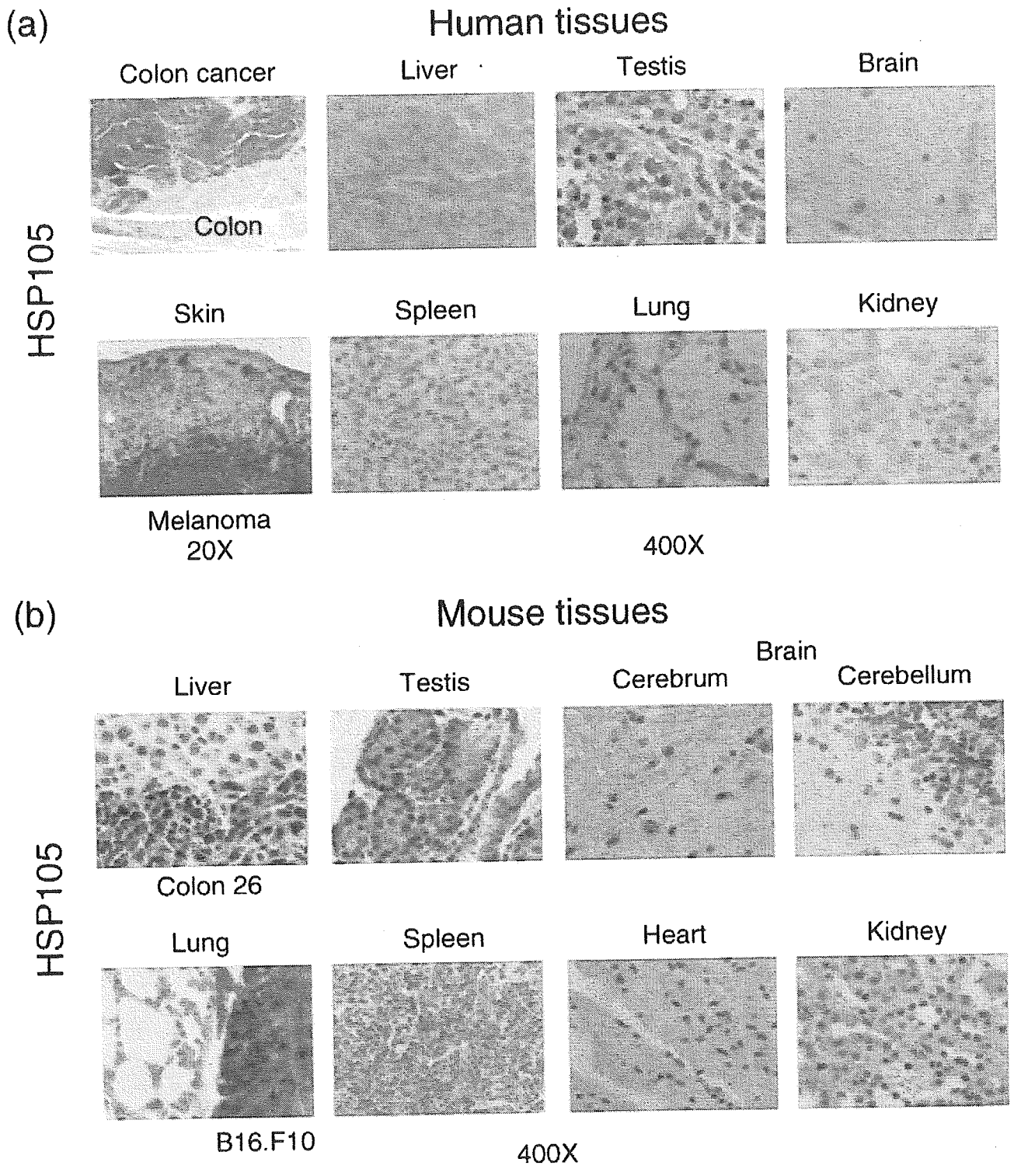

Fig. 1. Expression of the HSP105 protein, a candidate for immunotherapy for CRC and melanoma, in human and mouse tissues and cells. Expression of HSP105 protein detected by immunohistochemical analysis in various (a) human and (b) mouse tissues. Objective magnification was 400× or 20×.

 doi: 10.1111/j.1349-7006.2005.00093.x

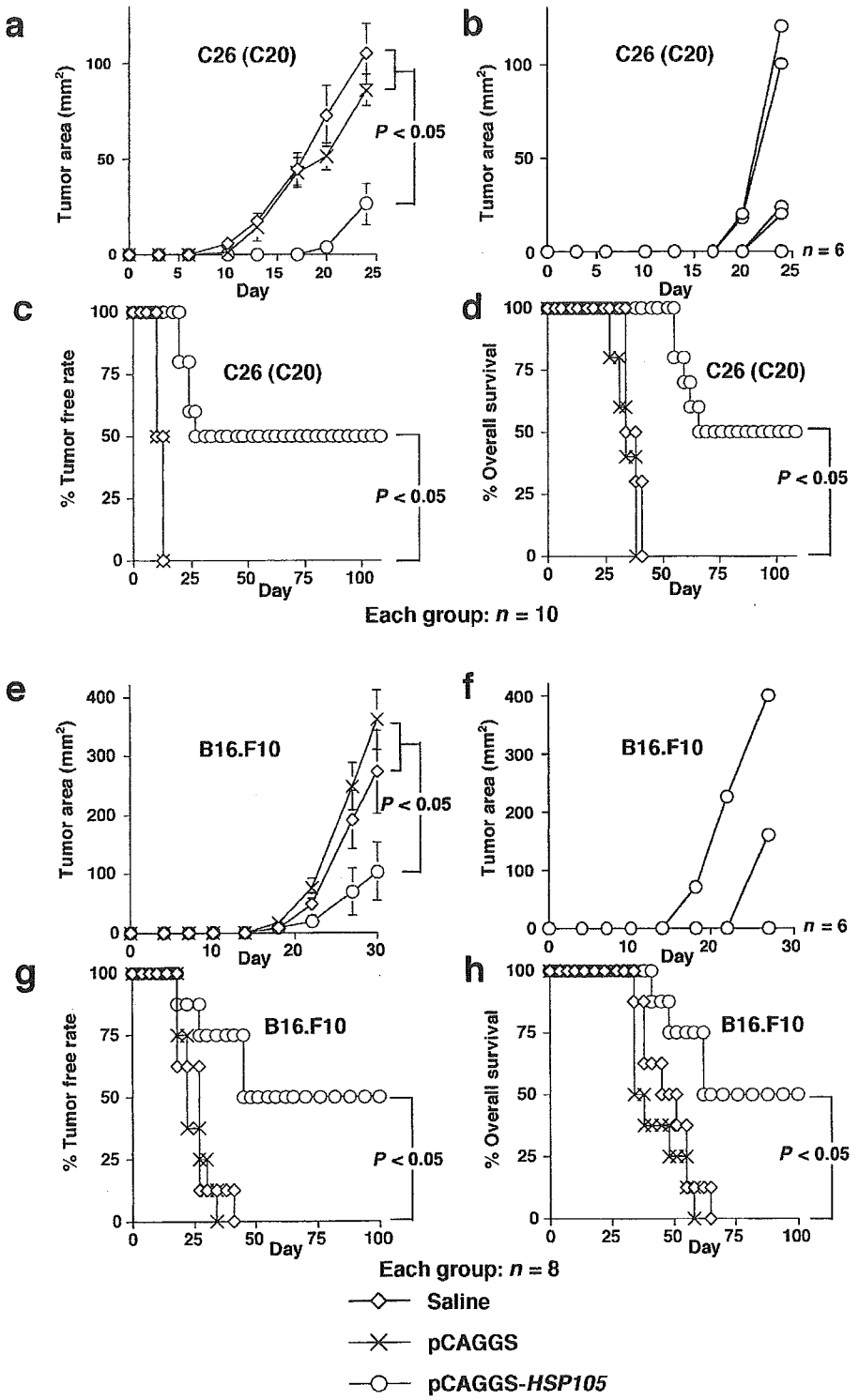

Fig. 2. Vaccination with *HSP105* DNA suppressed the growth of (a–d) C26 and (e–h) B16.F10 tumors in mice. Each group consisted of 10 (a–d) or eight (e–h) mice. (a,b,e,f) Suppression of the growth of HSP105-expressing C26 (a,b) or B16.F10 (e,f) tumors inoculated subcutaneously into mice vaccinated with *HSP105* DNA. The tumor area was calculated as the product of width and length. The result is presented as mean area of tumor ± SE, and we evaluated statistical significance using the unpaired *t*-test (a,e). Growth curves of 10 and eight individual tumors in the mouse group treated with pCAGGS-*HSP105* are presented in (b) and (f), respectively. (c,d,g,h) Percentage tumor free rate (c,g) and percentage overall survival (d,h) were calculated using the Kaplan–Meier method, and the statistical significance of differences between groups was evaluated using Wilcoxon's test.

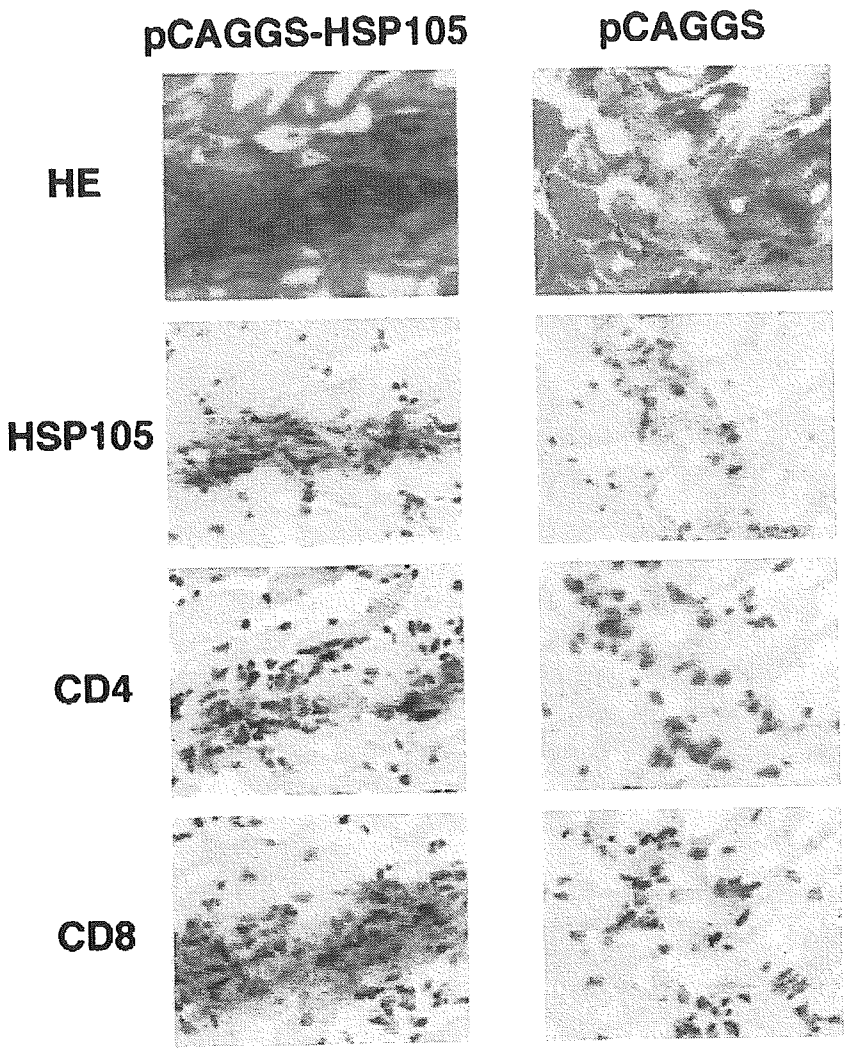

Fig. 3. Expression of HSP105 protein and infiltration of $CD4^+$ T cells and $CD8^+$ T cells in the *HSP105* DNA vaccine-injected sites. To observe HSP105 expression and infiltrating cells in muscles injected with the *HSP105* DNA vaccine, we carried out intramuscular immunizations with pCAGGS-DNA into the right anterior tibialis muscle, and with pCAGGS-*HSP105* DNA into the left anterior tibialis muscle in four mice. After 48 h, we killed the mice and studied their muscle tissue by using HE staining and histological analysis, and immunohistochemical analysis of HSP105, CD4, and CD8. Representative results are shown. Objective magnification was 400×.

lower than those in C26 (C20) tumor cells, which suggests a low risk of damage to normal tissue as a result of immune responses to the HSP105 antigen. To evaluate the risk of autoaggression by immunization against self-HSP105, the tissues of mice immunized with *HSP105* DNA were histologically examined. All mice were apparently healthy, and without abnormalities, suggesting autoimmunity for, for example, dermatitis, arthritis, or neurological disorders. The brain, liver, lung, heart, kidney, and spleen tissues of *HSP105*-immunized mice were critically scrutinized and compared with those of normal mice. These tissues had normal structure and cellularity for each of the two groups examined, and pathological changes caused by immune response, such as infiltrations of $CD8^+$ or $CD4^+$ T cells, or tissue destruction and repair, were not present (Fig. 4b). Although $CD4^+$ T cells and $CD8^+$ T cells infiltrated into the C26 tumor (Fig. 4a), infiltration of $CD4^+$ T cells or $CD8^+$ T cells was not observed in any of the normal adult tissues examined (Fig. 4b). These results indicate that T cells stimulated with the *HSP105* DNA vaccine do not recognize normal cells that express HSP105 at physiological levels.

Anti-C26 tumor adoptive immunity elicited by injection with $CD4^+$ T cells or $CD8^+$ T cells from *HSP105* DNA-vaccinated mice

Antitumor responses could be augmented by homeostatic T cell proliferation in the periphery, involving the expansion of T cells recognizing MHC/tumor antigenic peptide ligands.[21–23] To ascertain that the tumor rejections induced by *HSP105* DNA vaccination were mediated through the activation of $CD8^+$ T cells or $CD4^+$ T cells, in a homeostatic lymphocyte proliferation model, we subcutaneously inoculated BALB/c mice with C26 cells (3×10^4) 6 days after sublethal irradiation (5 Gy). We intravenously injected 1.5×10^7 whole spleen cells or 3×10^6 $CD8^+$ T cells, $CD4^+$ T cells, NK cells, or $CD8^-$ $CD4^-$ NK^- cells derived from each untreated or *HSP105* DNA-vaccinated mouse on day 3 before the tumor inoculation (Fig. 5a). Measurements of tumor size were continued for 22 days after inoculation with the tumor cells (Fig. 5b). Each group consisted of four mice. Inoculation with whole spleen cells or $CD8^+$ T cells, $CD4^+$ T cells, NK cells, or $CD8^-$ $CD4^-$ NK^- cells derived from untreated mice, and with NK cells, or $CD8^-$ $CD4^-$ NK^- cells derived from *HSP105* DNA-vaccinated

 doi: 10.1111/j.1349-7006.2005.00093.x

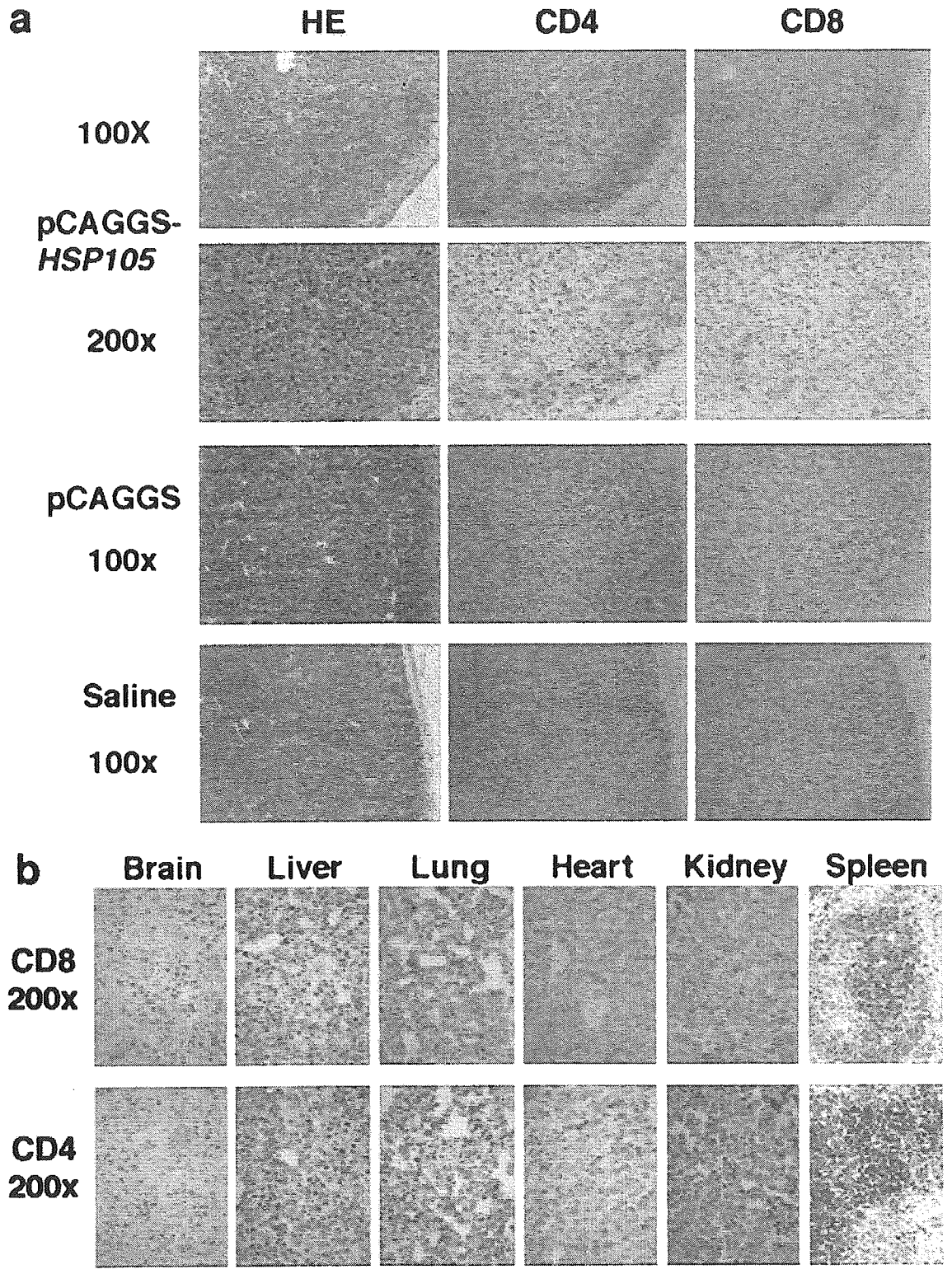

Fig. 4. Vaccination with *HSP105* DNA induced infiltration of both $CD4^+$ T cells and $CD8^+$ T cells into C26 tumors, but not into normal tissues. (a) Subcutaneous C26 tumors removed from two *HSP105* DNA-immunized mice, a saline-inoculated mouse, and a pCAGGS-immunized mouse that did not reject the tumor challenges were analyzed using immunohistochemical staining with anti-CD4 mAb and anti-CD8 mAb. (b) Normal tissues of mice vaccinated with *HSP105* DNA were histologically and immunohistochemically examined. Objective magnification was 200x. The spleen was used as a positive control for staining of both CD4 and CD8.